The discovery of a young radio galaxy at Z = 2.390 - Probing initial star formation at Z less than approximately 3.0

Windhorst, R.A.; Burstein, D.; Mathis, D.F.; Neuschaefer, L.W.; Bertola, F.; Buson, L.M.; ... ; Chambers, K.C.

THE ASTROPHYSICAL JOURNAL, 380:362–383, 1991 October 20

THE DISCOVERY OF A YOUNG RADIO GALAXY AT $z = 2.390$: PROBING INITIAL STAR FORMATION AT $z \lesssim 3.0$

ROGIER A. WINDHORST[1,2,3,4] DAVID BURSTEIN,[5] DOUG F. MATHIS,[2,3] AND LYMAN W. NEUSCHAEFER[2,3]
Department of Physics and Astronomy, Arizona State University, Tempe, AZ 85287-1504

F. BERTOLA[5]
Department of Astronomy, University of Padua, 35100 Padua, Italy

L. M. BUSON[5]
Astronomical Observatory, 35100 Padua, Italy

DAVID C. KOO[6]
University of California Observatories/Lick Observatory, Board of Studies in Astronomy and Astrophysics, University of California, Santa Cruz, CA 95064

KEITH MATTHEWS[1]
Palomar Observatory, Division of Physics, Mathematics, and Astronomy, California Institute of Technology, 320–47, Pasadena, CA 91125

PETER D. BARTHEL[7]
Kapteyn Astronomical Institute, P.O. Box 800, Groningen, 9700 AV, The Netherlands

AND

K. C. CHAMBERS
Sterrewacht Leiden, P.O. Box 9513, Leiden, 2300 RA, The Netherlands
Received 1991 January 3; accepted 1991 April 30

ABSTRACT

We present the discovery of a weak radio galaxy from the Leiden Berkeley Deep Survey at a redshift of 2.390, the faint optical and IR counterpart of the *steep-spectrum, compact* radio source 53W002. Its λ-dependent optical continuum morphology is compact with linear size $\sim$10–35 kpc ($H_0 = 50$, $q_0 = 0$). In redshifted Lyα, the galaxy is somewhat more extended ($\lesssim$67 kpc $\times$ 40 kpc). Its radio source is 7 times smaller than, and confined by, the Lyα gas. It shows alignment with the Lyα gas and the best seeing optical continuum images.

We present nine-band photometry (Lyα *UBgriJHK*) for the galaxy as well as surrounding objects. The source 53W002 is not variable on time scales of years, in either radio or optical. We compare its rest-frame UV continuum with *IUE* spectra of various nearby galaxies with relatively recent starbursts, and nearby active galactic nuclei (AGNs). The C IV/Lyα and N V/Lyα ratios suggest that 53W002 has a Seyfert 1–like AGN, and constrain the nonthermal component to be $\sim$35% of the observed UV continuum.

Several independent age estimates yield a consistent value of 0.25–0.32 Gyr: (1) its small 4000 Å break or UV-visual continuum amplitude compared with nearby galaxies; (2) a best model fit to the downturn of its UV spectrum below $\sim$2000 Å; (3) limits from the lack of detected stellar absorption features; (4) its total stellar mass (from its V- and K-band luminosity) compared with its SFR [from W_λ(Lyα, $z = 0$)]. These parameters together suggest that at $z = 2.390$, 53W002 had processed only a *few* times 10^{11} $M_\odot$ into stars, significantly less than most powerful radio galaxies have converted into stars at $z \sim 2$–3.8. Hence, star formation in 53W002 has proceeded slower, *and started* at a later epoch, than in the most powerful high-redshift radio galaxies.

The available data are consistent with 53W002 being a genuinely young (radio) galaxy seen at $z = 2.390$ during its first major starburst. It likely started forming *most* of its current stars at redshifts 2.5–3.0 (for $H_0 = 50$–100, $q_0 = 0.0$–0.5). This suggests that (radio) galaxies do not form the bulk of their stars coevally, but *start* doing so over a wide range of cosmic time.

Subject headings: galaxies: evolution — galaxies: stellar content — radio sources: galaxies — spectrophotometry

[1] Observations made at Palomar Observatory are part of a collaborative agreement between the California Institute of Technology and the Carnegie Institution of Washington.

[2] Optical observations obtained in part at the Multiple Mirror Telescope Observatory, a joint facility of the University of Arizona and the Smithsonian Institution.

[3] Optical observations obtained in part at the National Optical Astronomy Observatories, which are operated by the Association of Universities for Research in Astronomy, Inc., under contract with the National Science Foundation.

[4] Alfred P. Sloan Research Fellow.

[5] Partially based on observations obtained with the *International Ultraviolet Explorer* satellite, which is sponsored and operated by the United States National Aeronautics and Space Administration, by the Science Research Council of the United Kingdom, and by the European Space Agency.

[6] Presidential Young Investigator.

[7] Radio observations obtained in part at the National Radio Astronomy Observatory, which is operated by Associated Universities, Inc., under contract with the National Science Foundation.

1. INTRODUCTION

During the last decade, we made systematic deep radio-optical surveys of several selected areas at high Galactic latitude. The VLA and Westerbork were used to catalog 450 radio sources in the Leiden Berkeley Deep Survey (LBDS) down to microjansky levels (Windhorst, Mathis, & Neuschaefer 1990 and references therein). This sensitivity can trace galaxies with radio powers in excess of the break in the radio luminosity function ($\log P_{1.4} \gtrsim \log P^*_{1.4} = 25.0$ W Hz^{-1}) out to $z \gtrsim 5$, allowing the study of a complete sample of high-redshift galaxies with only weak active galactic nuclei (AGNs).

The Palomar 200 inch (5.08 m) Four-Shooter CCD array was used to obtain deep multicolor optical identifications (Windhorst, Dressler, & Koo 1987). Down to submillijansky levels, the radio source population is nearly *completely* optical identified down to $V = 27$ mag. Spectroscopic redshifts have been obtained for a representative sample of 175 weak LBDS radio galaxies as part of a long-term redshift survey in collaboration with R. Kron and A. Dressler (Kron, Koo, & Windhorst 1985; Windhorst, Dressler, & Koo 1987). The observed median redshift is ~ 0.35 for complete subsamples down to $V = 22$ mag, compared with $z_{\rm med} \sim 0.60$–0.75 from more limited statistics at the *medium* survey magnitude ($V \simeq 23.5$; Donnelly, Partridge, & Windhorst 1987; Windhorst et al. 1990). In this paper we present the discovery of the highest redshift weak LBDS radio galaxy 53W002 at $z = 2.390$.

For $V < 23.5$ mag, the spectra of extended (double-lobed) milijansky radio sources are indicative of passively evolving giant ellipticals (Kron et al. 1985; Oort et al. 1987), while the submillijansky radio source population is dominated by blue, actively star-forming galaxies with weak and narrow emission lines (usually [S II], Hα, [O III], Hβ, and [O II]; Kron et al. 1985; Windhorst et al. 1987). The latter most likely cause the upturn in the weak radio source counts (Windhorst et al. 1985). Only 3% of the LBDS radio galaxies possess the strong, high-ionization emission lines of Seyfert galaxies.

Investigations of powerful high-redshift $1 < z < 4$ radio galaxies recently revealed surprising properties (McCarthy 1988; Chambers 1989; Le Fèvre et al. 1988; Lilly 1988; Chambers, Miley, & van Breugel 1990). These most powerful high-redshift radio galaxies as part of a long-term redshift survey in collaboration with R. Kron and A. Dressler (Kron, Koo, & Windhorst 1985; Windhorst, Dressler, & Koo 1987). The observed median redshift is ~ 0.35 for complete subsamples down to $V = 22$ mag, compared with $z_{\rm med} \sim 0.60$–0.75 from more limited statistics at the *medium* survey magnitude ($V \simeq 23.5$; Donnelly, Partridge, & Windhorst 1987; Windhorst et al. 1990). In this paper we present the discovery of the highest redshift weak LBDS radio galaxy 53W002 at $z = 2.390$.

The recent search for very high redshift galaxies has been most successful among radio sources with the steepest radio spectra ($\alpha > 1$, $S_\nu \propto \nu^{-\alpha}$; Chambers, Miley, & van Breugel 1988, 1990). This has been explained in terms of possible selection effects induced by the P-α correlation and/or the radio K-correction (Kapahi & Kulkarni 1990; Windhorst et al. 1990). In the LBDS survey we tried to avoid this bias by getting fair samples of radio galaxies down to a given magnitude. For evolutionary studies, one would like to study the *same* kind of (radio) galaxy class at *all* cosmic epochs, even though such objects might look different at different redshifts. These galaxies should have *similar* space density, radio power, spectral index, and linear size of the radio source, *after* correcting for the likely effects of cosmic evolution in these parameters.

Because of their evolution, weak radio sources of comparable comoving space density (ignoring merging) will appear to evolve in radio power $P(z) \propto (1 + z)^{3.5 \pm 1}$ Windhorst 1984). For a galaxy like 53W002, the corresponding radio power and space density of its most likely present-day counterpart are $\log P_{1.4}(z = 0) \sim 25.5$ W Hz^{-1} and $\log \rho(z = 0) \sim 2.5$–$3.0$ Gpc^{-3}. Similarly, a weak $P - \alpha$ correlation and expected radio K-correction reduces its steep spectral index as *observed* at $z = 2.390$ to $\alpha \sim 0.74$ at $z = 0$ ($S_\nu \propto \nu^{-\alpha}$; Windhorst et al. 1990). The rather compact radio structure of 53W002 (< 7 kpc) corresponds to a linear size of ~ 150 kpc or less at $z = 0$, after correcting for likely size evolution [$\propto (1 + z)^{-2.5}$; Oort et al. 1987]. In other words, the four basic *radio* properties of 53W002 at $z = 2.390$—when reduced to $z = 0$—are like those of a radio galaxy with average spectral index, modest linear size, and radio power close to the Fanaroff-Riley (1974) break.

To be conservative, we will compare the far-UV rest-frame spectrum of 53W002 with a variety of nearby objects: (1) early-type active galaxies; (2) early-type galaxies whose spectrum is dominated by a recent burst of star formation (both from the *IUE* survey of Burstein et al. 1988); (3) nearby weak radio galaxies with low-ionization nuclear emission-line regions (LINERs) (Keel & Windhorst 1991); (4) nearby Seyfert galaxies; and (5) low-redshift quasars (types 4 and 5 both from Kinney et al. 1991).

Our multiwavelength observations of 53W002 are presented in § 2, along with a discussion of their reliability. Section 3 discusses the spectrum and wavelength-dependent morphology of 53W002. Section 4 compares its UV spectrum with that of nearby galaxies and AGNs with a wide range of star formation and nuclear activity. In § 5 we compare the far-UV SED of 53W002 with more powerful high-redshift radio galaxies, as well as with spectral evolution models. Our results are discussed and summarized in § 6.

Throughout this paper we assume a value of the Hubble constant of 50 km s^{-1} Mpc^{-1}, and $q_0 = 0$ in a Friedmann universe with $\Lambda = 0$.

2. RADIO, OPTICAL, AND NEAR-INFRARED OBSERVATIONS

2.1. *Target Selection*

The 175 LBDS radio galaxies thus far observed spectroscopically have $15 \lesssim V \lesssim 23.5$ mag and $0.023 < z < 2.39$. The highest measured redshift thus far is for the Westerbork radio source 53W002 (Windhorst, van Heerde, & Katgert 1984b,) presented in this paper. Only two other LBDS radio galaxies—out of 15 measured with $V \gtrsim 23$ mag—now have spectroscopic redshifts greater than 1.

2.2. *Radio Observations*

Table 1A summarizes the available radio data and Table 1B the optical data on 53W002. All radio synthesis observations were reduced in the standard way and calibrated with respect to 3C 286 (Baars et al. 1977). The source 53W002 was monitored with the Westerbork Synthesis Radio Telescope (WSRT) and the VLA during several years, and was *not* found to be variable at 1.41 GHz (Table 1A). Its 608.5–1412 MHz spectral index $\alpha^{0.6}_{1.4}$ is equal to 1.14 ± 0.07 (Windhorst & Oppe 1991). A 30 minute snapshot was taken with the new VLA 8.4 GHz receivers in 1990 March at 0".15 resolution (Fig. 1). Self-calibration yielded a higher dynamic range map to determine

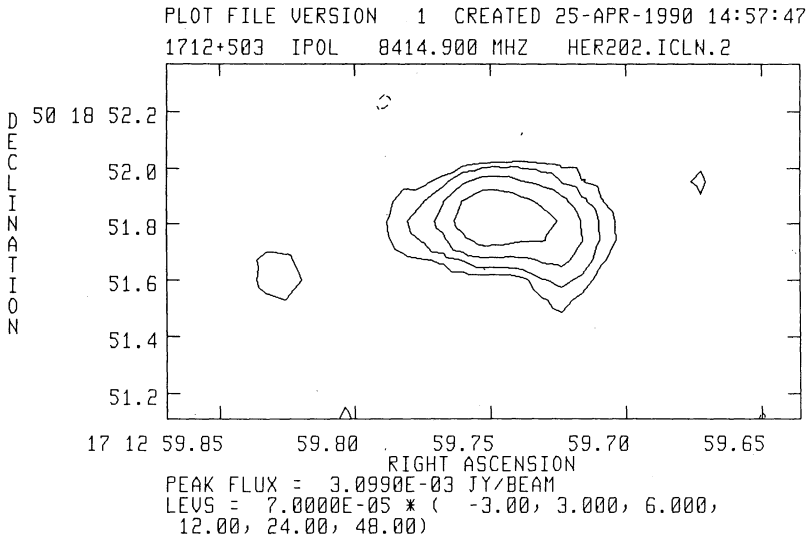

FIG. 1.—30 minute VLA A-array 8.4 GHz image of 53W002. The map has HPBW = 0.″15 and σ = 0.2 mJy. This is the highest resolution map available, and the *only* one is which 53W002 appears significantly extended (LAS ~ 0.″7). The radio source alignment with the Lyα image (Fig. 3, ΔP.A. $\lesssim 10°$) but is ~7 times smaller than the Lyα cloud.

TABLE 1A

LOG OF RADIO OBSERVATIONS OF 53W002[a]

Epoch	Telescope/ Instrument	HPBW of PSF (arcsec)	Frequency/ Bandwidth (MHz)	Flux (Error) (mJy)	LAS (arcsec)	P.A. (degrees)
1982.24.....	WSRT/DLB	27 × 36	0608.5/2.5	126.1(7.0)	9.0	136[b]
1980.52.....	WSRT/DLB	12 × 16	1412.0/10	50.1(4.3)	7.6	94[b]
1985.04.....	WSRT/DCB	12 × 16	1412.0/40	48.5(2.4)	9.4	21[b]
1985.08.....	VLA/A-array	1.40	1465.0/100	49.4(2.1)	<1.0	...[b]
1990.23.....	VLA/A-array	0.15	8414.9/100	5.3(0.4)	0.8	90

[a] Sources of data: 50 cm WSRT data from Windhorst & Oppe 1991; 21 cm WSRT data from Windhorst et al. 1984b and Oort & van Langevelde 1987; 20 cm VLA data from Oort et al. 1987. All other data from present paper.

[b] First three radio LAS (largest angular size) measurements were done with large FWHM and are overestimated. Their P.A.'s are also unreliable. Since the total 1.4 GHz fluxes measured with different beam sizes are consistent, it is not likely that these larger beam measurements picked up excess low surface brightness flux.

TABLE 1B

LOG OF OPTICAL/IR OBSERVATIONS OF 53W002

Epoch	Telescope/ Instrument	FWHM of PSF[a] (arcsec)	Filter λ_c/ FWHM (Å)	Flux (Error) (μJy)	FWHM (arcsec)	P.A. (degrees)
1989.52.....	SO 90/TI	1.60 ± 0.05	*U*(3600/530)	<0.78(2 σ)	<1.6	...
1988.91.....	Shane/UV-Schmidt	2.87 ± 0.10	*L*(4100/100)	6.81(1.0)[c]	4.0	96
1989.52.....	SO 90″/TI	1.81 ± 0.05	*B*(4420/1100)	2.17(0.30)	2.2	100
1988.60.....	MMT/spectrograph	2″ × 3″ aperture	*B*(4420/013)	1.50(0.30)	N.A.	90
1985.46.....	200/4-Shooter	1.65 ± 0.04	*g*(4950/900)	2.41(0.17)	1.9	111
1986.59.....	200/4-Shooter	1.33 ± 0.05	*g*(4950/900)	2.64(0.29)	2.0	114
1984.59.....	200/4-Shooter	1.60 ± 0.12	*r*(6550/850)	3.33(0.30)	1.7	99
1985.46.....	200/4-Shooter	1.39 ± 0.06	*r*(6550/850)	3.39(0.24)[d]	<1.4	...
1986.59.....	200/4-Shooter	1.43 ± 0.07	*r*(6550/850)	3.36(0.34)	1.5	73
1988.43.....	200/4-Shooter	1.14 ± 0.08	*i*(8080/1550)	4.06(0.31)	1.2	119
1990.59.....	200/IR-CAM	1.4	*J*(12600/1850)	8.7(1.1)	<1.4	...
1990.59.....	200/IR-CAM	1.1	*H*(16400/2800)	12.0(2.2)	<1.1	...
1990.59.....	200/IR-CAM	1.4	*K*(22200/3900)	13.9(2.4)[d]	1.9	93

[a] Equivalent circular FWHM of best-fit elliptical Gaussian averaged over about five PSF stars, plus rms error in this quantity.

[b] Equivalent circular FWHM of best-fit elliptical Gaussian to *observed* image, and *deconvolved* P.A. (using Wild 1970). The *deconvolved* FWHM values are discussed in § 3.2.

[c] To increase signal-to-noise, the two Lyα images of 1988 August and 1989 March were averaged (Fig. 3).

[d] This *r* exposure is the only one out of eight optical exposures that shows another $r = 24.69 \pm 0.26$ mag object 4″ due west. In *K*-band image, ~0.5 mag excess flux is seen when the aperture is similarly enlarged ~4″ to the west (Fig. 5). This flux is uncertain because of the high sky levels in *K*, falls beyond the apertures used for the other eight filters, and is therefore not included in Tables 1B and 4.

its integrated flux and search for low surface brightness extensions. The 1412–8415 MHz spectral index is 1.24 ± 0.04, and the *mean* 0.61–8.41 GHz spectral index is 1.21 ± 0.03.

In all maps, 53W002 was detected with peak signal-to-noise exceeding 35–300. However, the surface brightness sensitivity in these maps is not necessarily sufficient to detect any diffuse FR I radio structures at $z \gtrsim 2$ because of the $(1 + z)^4$ surface brightness dimming, especially when deep surveys approach the natural (i.e., resolution-independent) confusion limit (Fomalont et al. 1991).

2.3. *Astrometry*

About 25 primary AGK 3 standards—corrected for proper motion—were used to get a stable astrometric solution from a deep Palomar 48 inch (1.2 m) Schmidt plate taken at the same epoch as the CCD frames (Windhorst, Kron, & Koo 1984a). Typically 6–10 unsaturated secondary standards are available in the Four-Shooter chip, resulting in random errors of $\sim 0''.4$ and systematic errors less than $0''.3$. All 53W002 images were resampled onto the average Four-Shooter scale of $0''.335$ pixel^{-1}. Table 2 summarizes the astrometry for objects in the field. Stars C and D are secondary standards visible on Figure 2. Star D is a double (~ 18.5 mag with a ~ 21 mag star a few arcseconds due north) and has to be treated with care as an offset star.

Table 2 shows that the weighted mean over the five radio positions is known to a fairly high formal precision. The absolute VLA and WSRT position calibrators are believed to be accurate to within $0''.1$–$0''.2$. The core of the proposed optical identification of 53W002 differs from the radio position by 2.0

TABLE 2

ASTRONOMY OF OBJECTS SURROUNDING 53W002

Name	X	Y[a]	R.A.(1950.0)	Decl.(1950.0)	Approx V-mag[b]	Comments
			Radio			
53W002	...	...	$17^h12^m59^s.76$ (0.07)	$+50°18'51''.7$ (1.0)	...	WRST 0.61 GHz
53W002	...	...	17 12 59.71 (0.04)	+50 18 51.7 (0.5)	...	WRST 1.41 GHz
53W002	...	...	17 12 59.91 (0.06)	+50 18 51.8 (0.4)	...	WSRT 1.41 GHz
53W002	...	...	17 12 59.76 (0.01)	+50 18 51.6 (0.1)	...	VLA-A 1.46 GHz
53W002	...	...	17 12 59.755 (0.01)	+50 18 51.80 (0.1)	...	VLA-A 8.41 GHz
Adopted	296.9	253.2	17 12 59.758 (0.007)	+50 18 51.70 (0.07)	...	Weighted mean radio position
			Optical			
53W002	294.8	252.5	$17^h12^m59^s.83$ (0.04)	$+50°18'51''.3$ (0.4)	22.80	Core of optical identification deepest CCD frame
Star C	327.8	174.1	17 12 58.64 (0.04)	+50 18 24.7 (0.4)	17.0	Astrometric standard 29".0 SW, P.A. = 23
Star D	359.5	240.7	17 12 57.55 (0.04)	+50 18 47.5 (0.7)	18.5	Unequal double star 22".2 W, P.A. = 79
Star 1	312.6	468.8	17 12 59.25 (0.04)	+50 20 03.9 (0.4)	21.47	Photometric transfer star (K2 III?)
Star 2	182.5	260.6	17 13 03.76 (0.04)	+50 18 54.1 (0.4)	20.30	Photometric transfer star (F0 sd)
Star 3	161.9	158.8	17 13 04.45 (0.04)	+50 18 20.0 (0.4)	19.94	Photometric transfer star (F4 sd)
Star 4	355.7	081.7	17 12 57.68 (0.04)	+50 17 54.1 (0.4)	21.24	Photometric transfer star (K0 III?)
Star 5	359.4	193.5	17 12 57.57 (0.04)	+50 18 31.6 (0.4)	20.21	Photometric transfer star (F5 sd)
Object 1	407.7	207.4	17 12 55.88 (0.04)	+50 18 36.2 (0.4)	22.95	Foreground star
Object 2	387.8	284.5	17 12 56.59 (0.04)	+50 19 02.1 (0.4)	22.50	Low surface brightness object
Object 3	328.7	207.9	17 12 58.64 (0.04)	+50 18 36.4 (0.4)	22.86	Low surface brightness object
Object 4	328.9	269.8	17 12 58.64 (0.04)	−50 18 57.2 (0.4)	24.34	Very faint compact object
Object 5	311.7	269.9	17 12 59.25 (0.04)	+50 18 57.2 (0.4)	23.61	Low surface brightness object; compact core
Object 6	303.3	262.0	17 12 59.54 (0.04)	+50 18 54.6 (0.4)	22.0	Foreground star 4".1 NW
Object 7	269.2	278.7	17 13 00.73 (0.0)	+50 19 00.2 (0.4)	22.50	Low surface brightness object

[a] CCD X and Y (in pixels) measured from the stacked 3000 s Four-Shooter exposure with $0''.3350$ pixel^{-1}.

[b] V-magnitude only approximate for astrometric standards, and otherwise derived from the color transformations described in the Appendix.

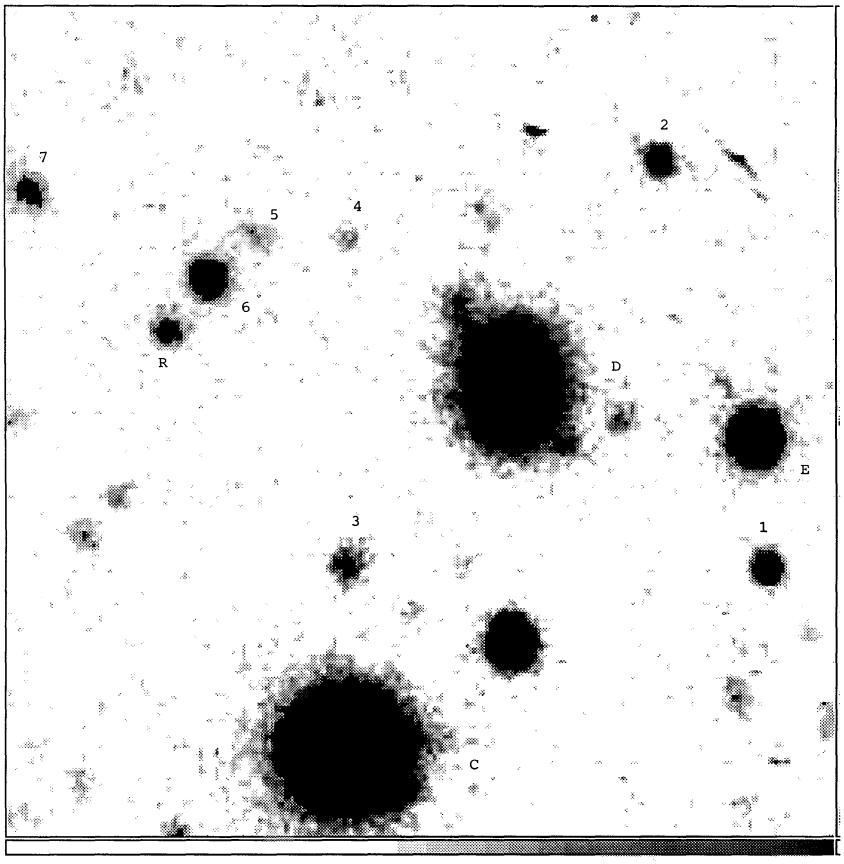

FIG. 2.—3000 s Four-shooter exposure (sum of 1500 s in both Gunn g and r). The displayed part is 52″ × 52″, and seeing in the stack is 1.″45 (FWHM). The image reaches a limiting magnitude of $V \sim 25.5$. The radio galaxy 53W002 is labeled "R" and is located at R.A.(1950) = $17^h12^m59^s.83$, decl.(1950) = +50°18′51.″3. Other surrounding objects are labeled as in Table 2. Note the compact appearance of 53W002 in the continuum, which has deconvolved FWHM ~1″.

σ. This decreases to 0.8 σ when systematic astrometry errors are accounted for (Windhorst et al. 1984a). The radio source lies well within the contour of the Lyα image (Fig. 3) which is thus considered the correct optical identification.

2.4. *Spectroscopy*

Optical spectra were taken with the Mayall 4 m Cryocam and the MMT red and blue spectrographs. The "blue channel" observations used a 300 line mm^{-1} grating (blazed at 4800 Å) and a dual 2″ × 3″ slit at P.A. = 90°, covering 3000–7800 Å at ~12 Å resolution. Internal flats and wavelength calibration exposures bracketed each object exposure in air mass. Wavelength calibration was accurate to ~1 Å, increasing to a few angstroms below 3500 Å. The spectra were fluxed with the Gunn standards BD +17°4708 and Feige 34, and corrected for atmospheric extinction. After wavelength calibration, the many 900 s pairs of sky and object + sky integrations were rebinned to a common wavelength scale and co-added with weights proportional to the inverse of the object + sky variance. To increase signal-to-noise ratio on weak lines, we smoothed the spectra with boxcars of n × 2.5 Å. The final unsmoothed resolution was ~13.5 Å FWHM, indicating that stacking of the many exposures somewhat broadened the lines. The flux-calibrated MMT spectra are given in Figure 4*a* (unrebinned observed frame) and Figure 4*b* (rest frame with a 10 Å boxcar to increase signal-to-noise). They are a sum of 14,440 s in 1988 June and 14,400 s in 1988 September. The difference spectrum between the two runs has a baseline of essentially zero with a somewhat λ-dependent rms noise (tracing the quality of the sky subtraction).

CCD spectra of 8 hr each were obtained at the 4 m Mayall Crycocam and the MMT red spectrograph to cover $\lambda \gtrsim 5000$ Å. The CCD read noise made the dark part of the sky in these exposures inferior in quality to the MMT Reticon spectra, and could only be used to confirm the detection of C IV, as well as marginal C III] and C II] (see Table 3).

The absolute flux calibration may have wavelength-dependent systematics, since a neutral density filter was used to measure spectroscopic standards. Absolute spectrophotometry is also compromised because some of the galaxy light will fall outside the 2″ × 3″ aperture of the MMT blue spectrograph (used at P.A. = 90°). Given the excellent offset pointing of the MMT ($\lesssim$0.″25 from our secondary stars with 0.″4 positional accuracy), and the fairly compact continuum morphology of 53W002 ($\lesssim$2.″0; § 3.2), we estimate that not more than ~20% of the light was lost in 1.″1 seeing. At redshifted Lyα, 53W002 is 5 × 3″ across at P.A. = 90°, but since most of the Lyα flux comes from the central core (§ 3.2), about 20%–30% of the Lyα flux may have been lost in the MMT aperture. Table 3 summarizes the emission lines in the spectra (Fig. 4*b*), as discussed in §§ 3.1 and 4.2.

2.5. *Optical/IR Imaging and Photometry*

2.5.1. *Photometric Technique*

All imaging data were initially reduced in the standard fashion, which includes debiasing, removal of the dark-current

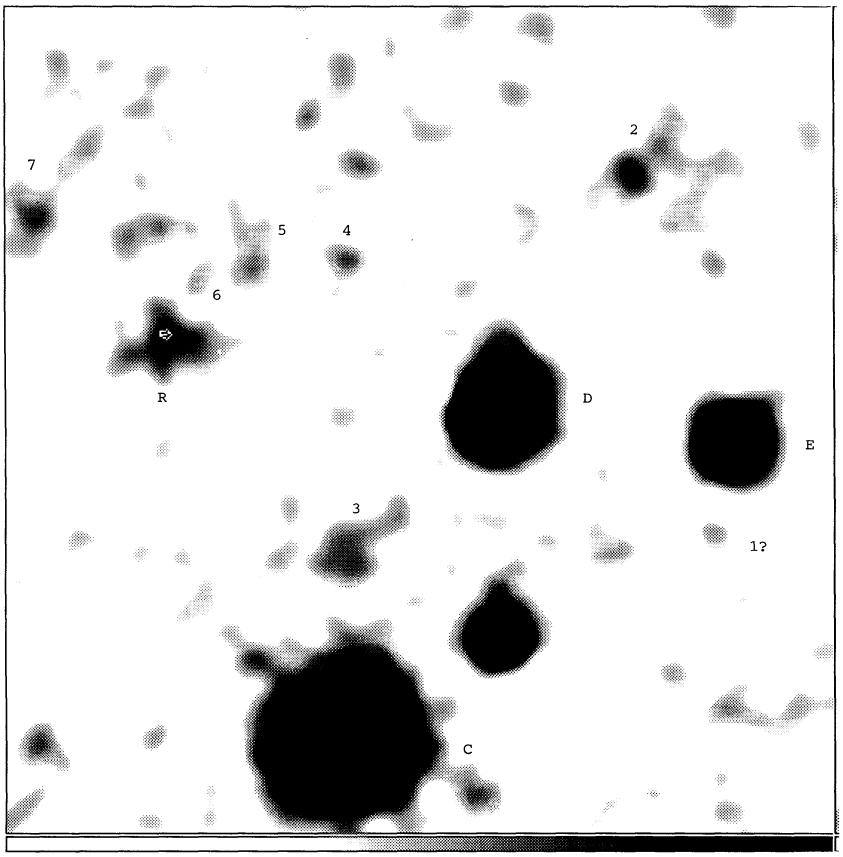

FIG. 3.—15,000 s narrow-band exposure in redshifted Lyα with the Shane 3 m and the Lick UV-Schmidt camera. The filter response was centered at 4100 Å with 100 Å FWHM. The displayed part is 52″ × 52″, and seeing in the stack is 2.″86 (FWHM) after Gaussian smoothing with FWHM = 0.″67. The image reaches AB(4100 Å) ~ 24.5 mag. All objects are labeled as in Fig. 2. The white overlay is the 8.4 GHz radio contour from Fig. 1, which is ~7 times smaller than the Lyα cloud.

TABLE 3

CHARACTERISTICS OF 53W002's SPECTRUM

λ_{obs} (Å)	Line Identification	λ_{rest} (Å)	z	W_λ (Å)	σ_v (km s^{-1})	Comments/Reliability
			Possible Emission Lines[a]			
4117.....	Lyα	1216	2.386	80	590	Possibly Lyman forest at short λ
4206.....	N v	1240	2.392	26	510	Clearly distinct from Lyα
5248.....	C iv	1549	2.388	33	670	Broader than Lyα
5560.....	He ii	1640	2.39:	...	...	Lost under night-sky 5577
6147.....	Si ii	1813	2.391	~33	<340	Possible
6478.....	C iii]	1909	2.393	≲23	<350	Lost in red part of MMT sky; also marginal in KPNO Cryocam
7880.....	C ii]	2326	2.388	...	...	Beyond MMT big blue sensitivity; marginal in KPNO Cryocam
			Limits to Possible Absorption Features[b]			
3092.....	Lyman discontinuity	912	...	...	...	Too close to atmospheric cutoff
4437.....	Stellar Si ii, Si iii	1304	...	< −5	...	Questionable
4728.....	Stellar Si iv	1399	...	< −5	...	Questionable
4814.....	Stellar Si ii blend	1426	2.38:	≲ −10	<680	Possible, also in M87
5037.....	Stellar Si i, Si ii	1478	2.41:	≲ −7	<350	Possible, also in M87
5469.....	Stellar Fe ii, Sr ii	1613	...	< −7	...	Questionable
6248.....	Stellar	1841	...	< −13	...	Questionable; in M87 on *IUE* fixed pattern noise?

[a] The average redshift deduced from the four believable emission lines is $z = 2.390 \pm 0.003$.

[b] Wavelengths of possible (inter)stellar absorption features were taken from Underhill 1982 and Prinja 1990. Some lines are blends, and their weighted rest-frame wavelengths are uncertain.

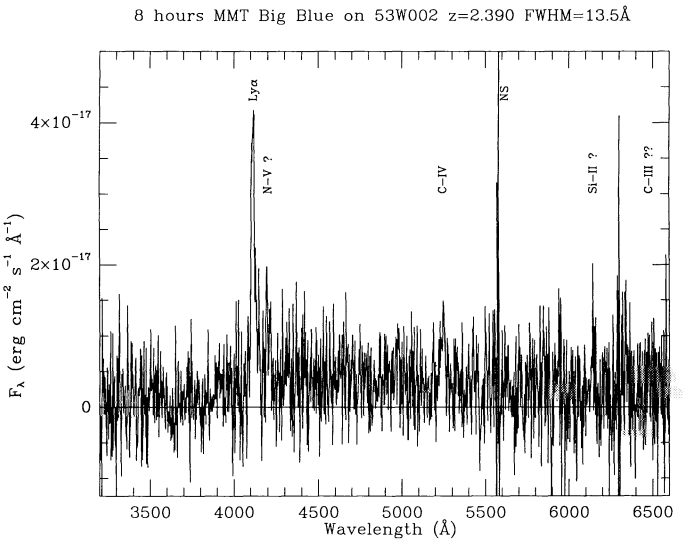

FIG. 4*a*

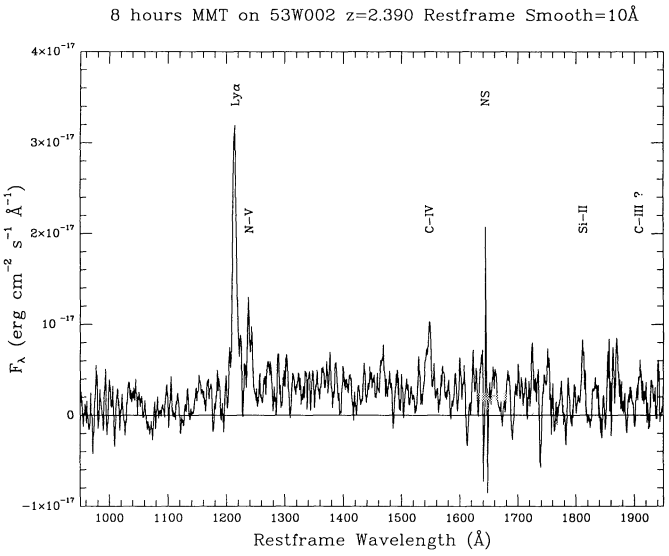

FIG. 4*b*

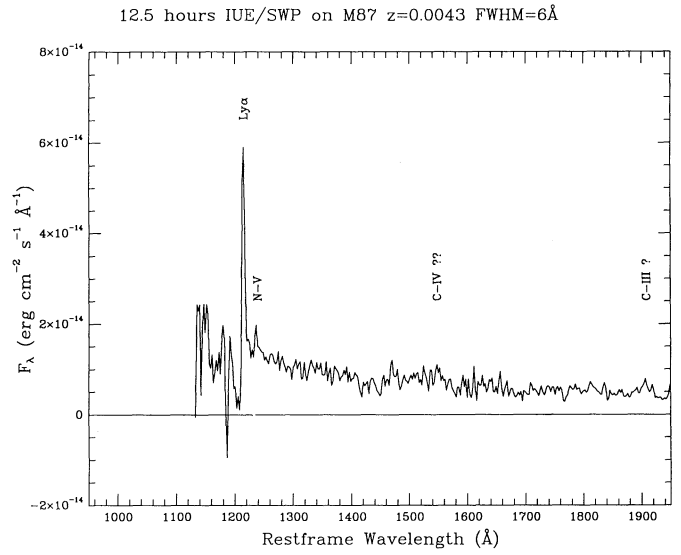

FIG. 4*c*

FIG. 4.—(*a*) 8 hr MMT spectrum of 53W002 in the observed frame. Resolution in the final stack is 13.5 Å, and the spectrum is displayed with its *original* 2.5 Å pixels. Positions of (possible) emission-line identifications are indicated. "NS" indicates poor night-sky subtraction at 5577 Å. (*b*) 8 hr MMT spectrum of 53W002 in the rest frame. After smoothing with a 10 Å boxcar to increase signal-to-noise, the resolution is 16.8 Å. Positions of (possible) emission-line identifications are indicated. (*c*) 12.5 hr *IUE* SWP spectrum of M87 (rest frame with $z = 0.0043$). Resolution is 6 Å. Positions of (possible) emission lines are indicated.

pattern, and flat-fielding against an iteratively averaged dome flat over the run (to increase signal-to-noise on the sky and reject outliers). Because Gunn filters are relatively narrow—and avoid most of the night-sky lines which generate fringes in the CCD—the remaining Four-Shooter systematics turn out to be *additive* low spatial frequency gradients that amount to a few percent of sky corner to corner (Neuschaefer, Windhorst, & Dressler 1991; Mathis, Neuschaefer, & Windhorst 1990). They were removed via a low-order spline surface fitted to an iteratively filtered grid of modal sky values (Mathis 1991).

After this standard processing, all images were resampled onto *one* common grid. Object photometry is then done with *identical* apertures (typically 11^2–16^2 pixels) in *each* band. Circular or rectangular object apertures are selected so as to minimize the enclosed sky, but to include ~95% or more of the object light visible in the highest contrast display of the best surface brightness sensitivity image ($\lesssim$28.0 mag arcsec^{-2}). In all bands, we used *empty* sky boxes of order 32^2–45^2 pixels. Sloped planes were fitted to these boxes to remove any remaining (linear) sky gradients. The spline + plane fitting routines were Monte Carlo tested, showing that they remove large-scale gradients to within $\sim 2 \times 10^{-4}$ of sky and numerical systematics within less than 5×10^{-5} (Mathis 1991). The resulting fluxes are thus nearly total magnitudes. Because we have identical sky boxes in all filters, the *colors* should be largely free of systematics.

2.5.2. *Four-Shooter Imaging and Photometry in Gunn gri*

Deep images were taken with the Palomar 200 inch Four-Shooter CCD array from 1984–1988 (Fig. 2). Table 1B lists the individual measurements at various epochs. The time-averaged nine-band photometry for 53W002—as well as for other surrounding faint objects–is given in Table 4. The average Gunn magnitudes of 53W002 are $g = 22.89 \pm 0.06$, $r = 22.78 \pm 0.05$, and $i = 22.68 \pm 0.08$. All listed errors are the inverse of the signal-to-noise ratio of the detection *only*, and reflect the combined uncertainties of photon statistics (object + sky) *plus* sky interpolation underneath the object. They do not include the (generally much smaller) zero-point error in transferring to the Oke & Gunn (1983) flux scale (§ 2.6).

2.5.3. *UB Imaging and Photometry*

We imaged 53W002 in Johnson *U* and *B* through long integrations at the Steward 90 inch (2.3 m) telescope. Zero-point calibration was bootstrapped as described in § 2.6. The resulting continuum *B*-magnitude is 23.30 ± 0.14, while in *U* we set a 2 σ upper limit of 23.1 mag. The flux at 4400 Å through the MMT blue spectrograph is 23.7 ± 0.2 mag, consistent with the Steward measurement minus the ~20%–30% light missed by the 2″ × 3″ spectrograph aperture (§ 2.4).

2.5.4. *Imaging and Photometry in Redshifted Lyα*

Two narrow-band exposures (7000 s in 1988 August and 8000 s in 1989 March) were obtained of 53W002 with the

TABLE 4

PHOTOMETRY OF OBJECTS SURROUNDING 53W002

Name	Gunn g (mag)	$(U-B)$ (mag)	$(4100-B)$ (mag)	$(B-g)$ (mag)	$(g-r)$ (mag)	$(r-i)$ (mag)	$(i-J)$ (mag)	$(J-H)$ (mag)	$(H-K)$ (mag)	Comments
53W002	22.89	> -0.2[a]	-1.17	$+0.41$	$+0.11$	$+0.10$	$+2.0$	$+0.8$	$+0.7$	Radio galaxy; $z = 2.39$;
	(0.06)		(0.18)[b]	(0.15)	(0.08)	(0.09)	(0.3)	(0.4)	(0.4)	extended in Lyα
Object 1	23.53	> -1.3	$> +1.0$	$> +0.9$	$+1.54$	$+1.16$	...	...	...	M5 star (III?);
	(0.14)				(0.14)	(0.04)				Hδ absorption
Object 2	22.75	$+0.1$	$+0.21$	$+0.13$	$+0.04$	$+0.46$	...	...	...	No 4100 Å excess
	(0.06)	(0.4)	(0.22)	(0.13)	(0.08)	(0.09)				or Hδ absorption
Object 3	23.21	> -0.5	-0.48	$+0.42$	$+0.44$	$+0.23$	...	...	...	Low surface brightness; possibly
	(0.10)		(0.30)	(0.20)	(0.12)	(0.10)				4100 Å excess
Object 4	24.27	> -1.0	-0.2	-0.1	-0.6	$+0.1$	...	...	...	No 4100 Å excess
	(0.22)		(0.4)	(0.3)	(0.4)	(0.4)				or Hδ absorption
Object 5	23.72	-1.7	-0.34	$+0.76$	$+0.32$	$+0.50$	> -0.2	...	...	Low surface brightness; compact
	[0.12]	[0.4]	[0.30]	[0.30]	[0.16]	[0.13]				core; $>3\ \sigma$ variable
Object 6	22.87	> -0.3	$> +1.4$	$+0.55$	$+1.21$	$+0.48$	$+1.78$	$+1.30$	$+0.57$	K6–7 III star;
	(0.07)			(0.17)	(0.07)	(0.04)	(0.09)	(0.11)	(0.22)	Hδ absorption
Object 7	22.91	> -0.0	$+0.04$	$+0.16$	$+0.33$	$+0.19$	...	...	...	No 4100 Å excess
	(0.08)		(0.24)	(0.18)	(0.09)	(0.09)				or Hδ absorption

[a] All upper limits are $2\ \sigma$.

[b] All listed optical/IR errors were derived from the inverse signal-to-noise ratio of the detection and do *not* include any uncertainties in the magnitude scale. The latter are small compared with the random errors, and are 0.3 mag in U, 0.1 mag in Lyα and B, 0.05 mag or less in Gunn *gri*, and 0.05 mag in Johnson JHK.

Shane 3 m UV-Schmidt camera. Redshifted Lyα was best matched through a commerically available filter with a triangularly shaped transmission curve having $\lambda_c = 4100$ Å and FWHM = 100 Å. The data were taken under photometric circumstances, and the two images were consistent. To increase signal-to-noise, they were averaged and convolved with a 1 pixel Gaussian (Fig. 3). Their flux calibration was complicated by substantial Hδ absorption of the early-type standards in the filter. Through the Gunn *gri* photometry (Tables 2 and 4) we identified several F2–5F subdwarfs (which have $\lesssim 0.1$ mag Hδ absorption; Oke & Gunn 1983) to further refine the 4100 Å zero point (§ 2.6).

2.5.5. *IR Imaging and Photometry*

The radio source 53W002 was observed for several hours with the Palomar 200 inch InSb IR array in Johnson JHK. Integrations of typically 150 s were processed in the standard way, and then median filtered to remove high spatial frequency structures in the IR night sky. This process left some low spatial frequency gradients that were removed through iterative spline surfaces (§ 2.5.1). Inspection of successive iterations showed that the photometricity of the frames was not destroyed beyond the 10% level, except at the very edges of these small frames (58 × 62 pixels).

Object 6 in Table 4 is 4″ northwest of 53W002 and has the Lyα $UBgri$ colors of a K6–7 III star (see Fig. 6 and § 3.5). It was used to check the zero point in the K band. Its K-magnitude before and after splining is 17.53 ± 0.20. Its Gunn *gri* colors transform to Johnson $B-V = 1.6$ and $V \sim 22.0 \pm 0.2$. From the IR extension of the Gunn-Stryker library (S. E. Persson, 1986, private communication), we find that a K6–7 III star should have $V-K = +4.4 \pm 0.3$ mag, consistent with our K-band measurement.

Inspection of the individually splined IR images suggests that detection of 53W002 in H and K is not better than $3\ \sigma$ (see the JHK stack in Fig. 5). The object is fainter in J, which, combined with the more difficult sky subtraction in J, yields an upper limit. Our best-estimated IR array magnitudes for 53W002 are $J \lesssim 20.7$ ($3\ \sigma$), $H = 19.9 \pm 0.3$, $K = 19.2 \pm 0.3$. In interpreting these data, one must bear in mind that the systematics in the IR sky are much higher, and more difficult to handle, than in the Four-Shooter frames. It is possible that systematic errors are larger than the quoted rms error, and only repeated observations can tell. If anything, we believe that our photometric procedure may have overestimated the J and

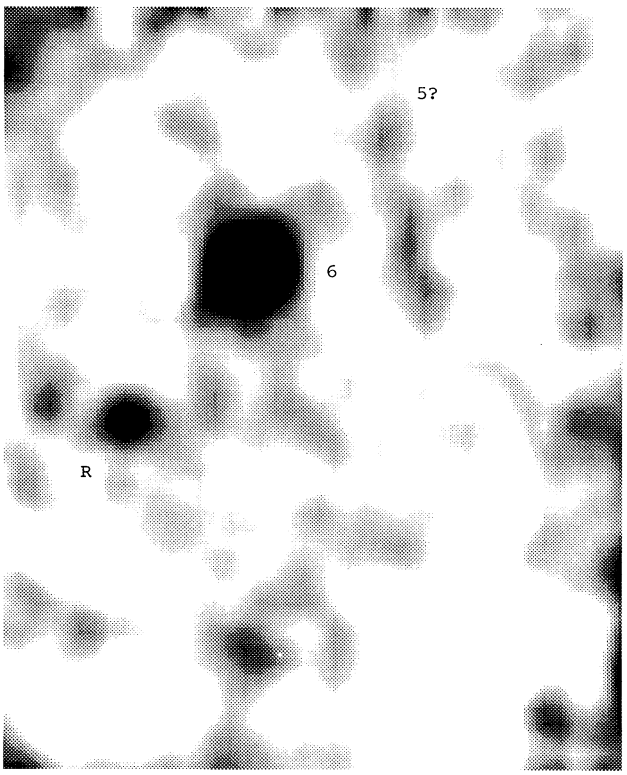

FIG. 5.—Stack of Johnson $J + H + K$ images taken with the Palomar 200 inch telescope and its IR camera. The displayed part is 13″ × 16″, and the stack has a stellar FWHM = 1.″30 after Gaussian smoothing with FWHM = 0.″335. This image reaches $H \sim 20.5$ mag. Objects are labeled as in Fig. 2. The radio galaxy is the faint object 4.″1 southeast of the bright ($K = 17.5$ mag) K star, and is only barely resolved (FWHM $\lesssim$ 1.″3).

H fluxes—so that both may be regarded as upper limits—and underestimated the K flux (see § 3.2 and notes to Table 1).

2.6. *Consistency of the Photometry*

All optical/IR calibrations were reduced to α Lyr or the primary Gunn standard BD +17°4708 (Oke & Gunn 1983). Some of the nights contributing to Johnson UB and Gunn gr were nonphotometric, and their zero point was bootstrapped from the photometric nights, using transfer stars 2, 3, and 5 with measured Gunn gri colors of F0–F5 subdwarfs, and stars 1 and 4 with colors of K0–K2 giants (Tables 2 and 4; Kent 1985; Oke & Gunn 1983). As described in the Appendix, all runs were reduced to the sensitivity of the photometric nights, which could be done to within 0.3 mag in U, 0.1 mag in B and Lyα, and better than 0.05 mag in Gunn gri. The photometric zero point in Johnson JHK is also known to within 0.05 mag.

From the AB-magnitudes of α Lyr and BD +17°4708 (Oke & Gunn 1983), and the observed slopes of 53W002's continuum, we derive the following Johnson BV and Mould RI magnitudes: $B \sim 23.3$, $V = 22.8$, $R = 22.5$, and $I \sim 22.1$ mag. The Appendix also summarizes the relevant color transformations between Gunn gri, Johnson BV/Mould RI, and photographic U^+J^+FN. These predict $BVRI$ magnitudes consistent with the above values to within 0.10–0.15 mag. In particular, the B-magnitudes estimated this way are consistent with the two measurements in § 2.5.3.

For comparison with the IUE spectra of nearby galaxies [given on a log $F_\lambda(\lambda)/F_\lambda(V)$ scale], the rest-frame $(1550 - V)$ color of 53W002 was calculated as follows: Interpolation in Table 1B yielded F_ν-continuum values at 5255 Å and 1.86 μm, corresponding to rest-frame 1550 and V, respectively. We find $F_\nu(1550)/F_\nu(5500) = 2.61$ μJy/12.8 μJy $= 0.20 \pm 0.06$ (see Appendix), most of the error arising from the uncertain sky subtraction in H and K. Combined with the wavelength ratio of 3.58 and the relative bandwidth of 2.8, we find $F_\lambda(5500) = 0.93 \pm 0.31$, or +0.07 mag. Hence, Figure 7 shows log $F_\lambda(\lambda)$ − log $F_\lambda(V)$ versus λ normalized at log $F_\nu(1550)$ − log $F_\lambda(V) = -0.03 \pm 0.13$ dex.

2.7. *IUE Observations of Nearby Active and Star-forming Galaxies*

In a continuing program to better define the UV SEDs of early-type galaxies, IUE exposures have been obtained for a variety of nearby galaxies (Burstein et al. 1988). These constitute a useful comparison sample and include quiescent, radio, and actively star-forming galaxies. Recently, we obtained a 748 minute short-wavelength camera exposure of M87 (SWP 32871) with IUE. This turned out to be one of the highest quality UV spectra of a nearby low-luminosity radio galaxy.

Usually, the high geocoronal Lyα flux saturates the IUE SWP detector, so that Lyα from nearby galaxies—redshifted by only 5–10 Å—cannot be detected. Fortuitously, this longest SWP exposure coincided with a period of weak geocoronal Lyα emission, so that Lyα from M87's center *was* visible on the redward wing of geocoronal Lyα (Buson, Bertola & Burstein 1990). The SWP spectrum was reduced in a line-by-line manner similar to the spectra of Burstein et al. (1988), which give details of this technique. M87's Lyα emission is centered on its nucleus and extends ~3″ from the center on the wing of saturated geocoronal Lyα. In order to obtain a quantitative measurement of M87's Lyα emission, an *average* profile was constructed along the spectrum using several scan lines at the edges of the IUE aperture, which correspond to regions of M87 without Lyα emission. This profile was expanded to match the full IUE aperture and then subtracted from the observed image. This procedure satisfactorily subtracted geocoronal Lyα, but also subtracted a fraction of the true M87 continuum. The latter was re-added into the final spectrum, which contains the total UV flux and only the intrinsic Lyα emission of M87.

2.8. *Galactic Absorption Correction*

No Galactic absorption correction was applied to the optical/IR photometry of 53W002, since the bootstrapping of our photometric zero points already takes out most of the reddening, and extinction is small in the Hercules field ($A_V =$ 0.05 mag; Burstein & Heiles 1982). The IUE spectrum of M87 has been corrected for Galactic extinction as in Burstein et al. (1988), using $A_B = 0.08$ mag and the analytic extinction model of Seaton (1979).

3. PROPERTIES OF 53W002 AND ITS SURROUNDINGS

3.1. *The Spectrum and Its Redshift*

Table 3 summarizes possible emission lines in the UV spectrum of 53W002 (see Figs. 4 and 4*b*). Solid line identifications are Lyα, N v, C iv, and possibly Si ii (given that the spectrophotometry in the red was compromised). He ii was too close to night-sky 5577 Å. The strongest emission line —Lyα—is in a dark part of the sky unaffected by night-sky lines and read noise. C iii] is questionable in Figure 4*b*, but was seen in a KPNO Cryocam spectrum, possibly along with some weak C ii]. The Cryocam are not reproduced, since their signal-to-noise ratio is low, and they were nonphotometric.

The redshift deduced from the three certain and one possible emission lines is $z = 2.390 \pm 0.003$. Limits to possible stellar absorption features (Table 3) are discussed in § 4.3.

3.2. *The Optical/IR Continuum and Lyα Morphology*

Figure 2 shows the sum of two 1500 s exposures in Gunn g and r with the Palomar 200 inch Four-Shooter CCD array, reaching a limiting stellar magnitude of $V \sim 25.5$ mag. The optical counterpart of the radio source 53W002—labeled "R"—is barely resolved, so that it was originally classified in our survey as a "faint quasar."

About five stars immediately surrounding the radio galaxy were used to construct an average point-spread function (PSF) to quantify 53W002's continuum extent. Over the small CCD region involved ($\lesssim$100 pixels), focus variations are small compared with the seeing FWHM. The PSF could be determined to within ~0.″05–0.″10 for each of the 11 continuum images (Table 1*B*). These PSF stars are also slightly extended as a result of guiding errors. Their "position angles" were consistent within 15°, *and different* from 53W002's optical image. Assuming elliptical Gaussian symmetry, we deconvolved 53W002's image in each bandpass with its *average* stellar PSF following Wild (1970).

Eight of the 11 continuum images in Table 1B indicate a slight extension (1.″2–2.″2) of the observed UV-optical continuum (with seeing FWHM in the range 1.″1–1.″8). The resulting *deconvolved* image FWHMs of 53W002 are less than 1.″6 in Johnson U, 1.″3 in B, 1.″2 in Gunn g, 0.″6 in r, 0.″4 in i, less than 1.″4 in Johnson J, less than 1.″1 in H, and 1.″3 in the K band. The decrease of deconvolved FWHM toward longer wavelengths appears larger than the errors reasonably allow. Apart from the better seeing at the longer wavelengths, this may

suggest that 53W002 is somewhat larger in its restframe *UV continuum* than for $\lambda_{rest} \gtrsim 4000$ Å. This is consistent with a more extended stellar population or a scattered light cone from a hidden AGN in the UV/blue, and a more compact, older stellar population or a steep-spectrum AGN dominating longward of 4000 Å.

The largest angular size of the deepest continuum image is about twice the image FWHM, or $\sim 2\farcs6$ down to $V \lesssim 28.0$ mag arcsec^{-2}. The deconvolved sizes correspond to less than 10 kpc in the far-red to ~ 35 kpc in the UV/blue at $z = 2.390$. The $(1 + z)^4$ dimming reduces the average surface brightness of a galaxy bulge at $z = 2.390$ down to ~ 28 mag arcsec^{-2}, close to our detection limit. Hence, down to a given isophote, 53W002 *appears* smaller than it actually is (beyond the restframe 4000 Å break it appears smaller than the size of a *present-day* galaxy).

The best Gunn r image shows another $r = 24.69 \pm 0.26$ mag object 4″ due west of 53W002. Some ~ 0.5 mag excess flux is also seen in the K-band image when the aperture is similarly enlarged 4″ west (see Fig. 5). These are the *only* continuum exposures that show a possible multiple component. Since the deepest continuum images show no low surface brightness emission connecting to 53W002, it is not clear whether this other flux is physically related to 53W002.

The 15,000 s redshifted Lyα narrow-band exposure on the Lick 3 m telescope (Fig. 3) shows that 53W002 has high central surface brightness and is clearly elongated in Lyα (size $\sim 5'' \times 3''$ down to $B \sim 28.0$ mag arcsec^{-2}, or ~ 67 kpc $\times$ 40 kpc). However, surface photometry in the unconvolved Lyα image showed that more than 50% of the total Lyα flux actually comes from the *central independent pixel*, or more than 65% within the $2'' \times 3''$ MMT aperture (§ 2.4). This suggests that most of the Lyα flux may in fact come from the nucleus, consistent with constraints from the line ratios in § 3.6. Note that the Lyα peak flux within the $2'' \times 3''$ aperture MMT spectrum is 10.7 times the strength of the continuum (Fig. 4*b*), while the Lyα flux within the $5'' \times 3''$ aperture narrow-band filter is only 3.6 times stronger than the continuum (Fig. 8), because this filter has FWHM $\simeq 0.36 \times W_\lambda$(Lyα).

In conclusion, the optical continuum of 53W002 is more regular and smaller than that of the very large, clumpy high-redshift radio galaxies recently found in bright radio surveys. Its Lyα morphology is also more centrally concentrated.

3.3. *Alignment with the Radio Source*

The 3.4 cm map is the highest resolution radio map available, and the only one in which 53W002 is significantly resolved (FWHM $\sim 0\farcs5$ at P.A. $90° \pm 3°$; Fig. 1 and § 2.2). The radio source axis is thus aligned with the elongated Lyα emission-line nebulae (P.A. $96° \pm 5°$; Fig. 3). The average *deconvolved* P.A. of 53W002 in the (slightly) extended *continuum* images (§ 3.2) is 101° ($\sigma = 14°$), which is also aligned with the radio source (because of the compactness of 53W002, this is not visible in the gray-scale reproduction of Fig. 2). The *radio-optical continuum* P.A. difference is thus within the combined error, and we can exclude a radio-optical *continuum misalignment* of ΔP.A. $\gtrsim 30°$ at the more than the 2 σ level.

This result extends the "alignment effect" found in powerful high-redshift radio galaxies (Chambers et al. 1987; McCarthy et al. 1987; Chambers & McCarthy 1990) to lower radio powers. The observed largest angular size of the radio source (LAS $\sim 0\farcs7$) is somewhat smaller than the optical continuum (1″–2″) and clearly smaller than the Lyα image ($\sim 5'' \times 3''$). As noted in §§ 1 and 3.7, 53W002 has a radio power near the dividing line between the two common morphologies of steep-spectrum radio sources at low redshift. If 53W002 is an edge-brightened double (FR II), then the *detected* radio source angular size is a measure of the true radio source size. However, if 53W002 has edge-darkened morphology (FR I, like, e.g., M87), its weak radio lobes may not be detected because of the $(1 + z)^{-4}$ surface brightness. Its apparent radio size will depend on the flux density limit of the radio map, and may be significantly larger than the size observed in Figure 1.

Since about two-thirds of 53W002's optical-IR continuum is due to starlight (§§ 3.6 and 5.1), the radio-optical continuum alignment suggests that a jet may trigger star formation in weaker radio sources as well, just as it appears to do in the most powerful radio sources. Chambers (1989) discusses some consequences of jet-induced star formation in weak radio sources at high redshift.

In conclusion, while 53W002 is only one object, it suggests that at high redshifts the alignment effect may be present over a range of more than 100 in radio power, and thus may depend more strongly on redshift than on radio power. This is consistent with recent results from the brighter Molonglo survey (McCarthy et al. 1990a).

3.4. *Limits to Variability*

After all Four-Shooter runs were reduced to the sensitivity of the photometric nights, only object 5 (Table 4) turned out to be possibly variable on time scales of years, at the 4 σ level in Gunn r and the 1.5 σ level in Gunn g. Its $U - B$, $B - g$, $r - i$ and *average* $g - r$ colors are also unusual (see Fig. 6), as are the $g - r$ colors measured at the *same* epoch (a 3 σ color change in 1 year). On Figure 3, object 5 appears to have a compact core embedded in a fainter halo. It may be an AGN, not necessarily at the same redshift as 53W002, and *without* radio emission down to 0.1 mJy.

In contrast, the radio and Gunn gr fluxes of 53W002 (Table 1) show no evidence for variability on time scales of 1–4 yr (we could have detected 35% variations at the 3 σ level). Hence, the Seyfert 1–like nucleus of 53W002 discussed in § 3.6 apparently does not dominate its UV light through variable nonthermal contributions. These radio-optical data also preclude the possibility that 53W002 is gravitationally microlensed by the late K giant 4″.1 northwest (e.g., LeFèvre et al. 1988), producing object 5 as a secondary image on the opposite side (Fig. 2).

3.5. *Surrounding Objects*

The Lyα image (Fig. 3) shows several other very faint low surface brightness objects surrounding 53W002, which are barely visible in the 3000 second Four-Shooter continuum exposure (Fig. 2). Figure 6 shows their $(4100 - B)$ versus $(B - g)$ color-color diagram. Because the 4100 Å band is within the FWHM of the Johnson B band, this diagram can locate objects with significant emission or absorption at 4100 Å, albeit with large relative errors in $(B - g)$. A featureless power law ($F_\nu \propto \nu^{-\alpha}$) is indicated by the dotted line in Figure 6, with tick marks indicating integer values of α. Three different photometric filter systems contribute to Figure 6, as calibrated in the Appendix. The three crosses around $\alpha = 1.0$ are photometric transfer stars (F subdwarfs) whose Hδ absorption lines are expected to be about 0.10 mag fainter than the continuum (Oke & Gunn 1983). Objects 2, 4, and 7 are low surface brightness galaxies with no excess signal at 4100 Å. If they are at the same redshift as 53W002, their Lyα—and thus their star formation rate (SFR)—is that least 10 times smaller than 53W002. Objects 1 and 6 have the *UBgri* colors of M and K stars,

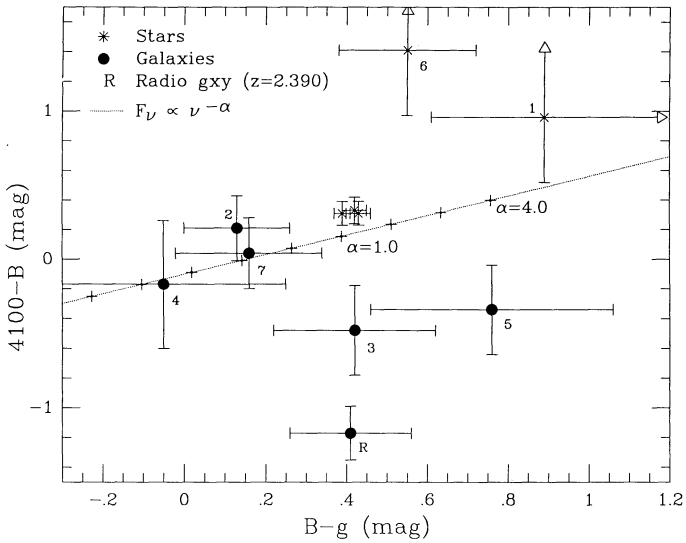

FIG. 6.—(4100 Å − *B*) vs. (*B* − *g*) color-color diagram for objects surrounding 53W002. The locus of featureless power-law spectra ($F_\nu \propto \nu^{-\alpha}$) is indicated by the dotted line with tick marks indicating integer values of α. The three crosses around α = 1 are F subdwarfs with mild Hδ absorption. Objects 2, 4, and 7 are flat-spectrum galaxies with no excess signal in Hδ or redshifted Lyα. Objects 1 and 6 are late-type stars with considerable Hδ absorption. Object 5 has a variable component on time scales of years. Next to 53W002, object 3 is the only other surrounding galaxy that possibly has an emission line redshifted into the 4100 band.

respectively, and have considerable (Hδ + metallic) absorption at 4100 Å. Object 5 has a compact core in its continuum that is possibly variable (§ 3.4).

In conclusion, apart from 53W002, object 3 is the only other galaxy that has fairly significant excess light in the 4100 Å narrow band. If this is redshifted Lyα, its W_λ would be about half as strong as 53W002 and would take four nights to confirm spectroscopically with the MMT. This illustrates how hard it is to find Lyα galaxy candidates at the same redshift as a known AGN. Such objects might be rare, because the more massive AGN could form most of its stars before the less massive surrounding members started forming.

3.6. *The Nonthermal Power-Law Contribution*

The Lyα line of 53W002 is fairly narrow in its peak (Fig. 4*a*), but possibly has an underlying weak broad-line component buried in the noise (Fig. 4*b*). Compared with 53W002, Lyα appears to be narrower in low-redshift, low-luminosity radio galaxies (e.g., Fig. 4*c*) and in the most powerful high-redshift 3CR radio galaxies (McCarthy 1991). C IV may have an underlying broad component as well, while the *observed* C IV/Lyα and N V/Lyα line ratios are unusual for H II regions. Hence, we need to address the fractional contribution of a nonthermal power law to its rest-frame UV continuum. We refer to this as $f_{1450}^{\rm AGN}$ at 1450 Å. With the average Gunn *g* flux of Table 1B, 53W002 has a luminosity of $L_{1450} = 10^{30.49}$ ergs s^{-1} Hz^{-1}. For plausible power-law spectral indices of 0.8–1.2 (Kinney et al. 1985), the *K*-correction to this value is about ±0.1 dex, which is otherwise just a scaling factor that does not affect the discussion below.

With this value of L_{1450} as upper limit, we use the *observed* (Baldwin) relations between W_λ(C IV), W_λ(Lyα), C IV/Lyα, and L_{1450} for low-redshift Seyferts and high-redshift quasars (Kinney et al. 1985, 1987, 1990; note that they use $q_0 = 1$) to constrain the nonthermal contribution of 53W002. Here we assumed that 53W002's C IV line comes *entirely from the AGN*, while Lyα has to be decomposed into a *broad-line AGN* component and a *narrow-line* component associated with the young stellar population. Since equivalent width is defined in terms of the *total* continuum, we require that the ratio of *observed* W_λ(C IV, $z = 0$) = 33 Å to that *predicted* by the Kinney et al. diagrams be consistent with the input value of $f_{1450}^{\rm AGN}$, which was found by iteration. The permitted range is $0.20 < f_{1450}^{\rm AGN} < 0.60$, with a maximum-likelihood value of $f_{1450}^{\rm AGN} = 0.35 \pm 0.15$. The C IV rest-frame equivalent width that 53W002 would have had with respect to its *AGN continuum alone*—W_λ(C IV, AGN)—then simply follows from the observed value W_λ(C IV, $z = 0$) divided by $f_{1450}^{\rm AGN}$: ≃33 Å/0.35 = 94 ± 25 Å.

The *total* Lyα rest-frame equivalent width that 53W002 would have had with respect to its *AGN continuum alone*—W_λ(Lyα, AGN)—must be determined differently, since the *observed* W_λ(Lyα, $z = 0$) = 80 ± 25 Å (Table 3)—measured with respect to its *total continuum*—will contain both AGN and starburst contributions. Given $f_{1450}^{\rm AGN} = 0.35 \pm 0.15$ and the above value of W_λ(C IV, AGN) = 94 Å, W_λ(Lyα, AGN) must follow in a self-consistent way from the observed W_λ(Lyα) and C IV/Lyα versus L_{1450} relations of Kinney et al. Both diagrams yield consistent results: W_λ(Lyα, AGN) ≃ 154 ± 15 Å. The observed value of W_λ(Lyα, $z = 0$) thus enters as a boundary condition, since the nonthermal contribution $f_{1450}^{\rm AGN}$ cannot be so large that its associated Lyα equivalent width—as predicted from the Baldwin relations—would exceed the observed value W_λ(Lyα, $z = 0$).

We can now decompose W_λ(Lyα, $z = 0$) into the AGN and starburst components. Analogous to the determination of W_λ(C IV, AGN), the Lyα component from the AGN *alone*—and measured with respect to the AGN continuum *alone*—would thus be ≃(35% ± 15%) × 154 Å ≃ 54 ± 23 Å. The remainder of the observed W_λ(Lyα, $z = 0$) = 80 ± 25 Å must be the narrow-line component associated with the starburst: 80 − 54 ≃ 26 ± 10 Å. The latter may be underestimated by less than 50% because the stellar continuum will have some Lyα in absorption if it is indeed primarily caused by late B stars (Fig. 8 and § 5). It is important to realize that, even though the *UV continuum* is *not* dominated by the AGN, about 68% (or 54 out of 80 Å) of the *observed* W_λ(Lyα, $z = 0$) *does* in fact come from the AGN. This is consistent with § 3.2, which showed that more than 50% of the total Lyα emission actually comes from the central independent pixel.

For the AGN component *alone*, we find the following line ratios for 53W002: C IV/Lyα ≃ 94 Å/154 Å = 33 Å/54 Å = 0.61, N V/Lyα = 26 Å/54 Å = 0.48, and C III]/C IV = 23 Å/33 Å = 0.70. All three are at the high end of the observed ranges summarized by Kwan & Krolik (1981), indicating a fairly luminous Seyfert 1. In § 5.1 we present several arguments that the nonthermal contribution to the continuum cannot easily exceed 50% at 1450 Å. With $f_{1450}^{\rm AGN} = 0.35 \pm 0.15$, the continuum luminosity from the AGN *alone* is log L_{1450} (W Hz^{-1}) = 30.0 ± 0.2. The boundary region between Seyfert 1 galaxies and QSOs occurs at log $L_{1450} \sim 30.6$, just brighter than the *total* observed continuum luminosity for 53W002 (log $L_{1450} = 30.49$). Hence, at $z = 2.390$ (the nonthermal component of) 53W002 did not quite reach a QSO–like continuum luminosity.

We verified these conclusions with the W_λ(C IV) versus M_{1550} diagrams of Wampler et al. (1984), Baldwin, Wampler, & Gaskell (1989), or Crampton, Cowley, & Hartwick (1990).

The 1550 Å AB flux of 53W002 (§ 2.6) corresponds to $M_{1550} = -24.65$ (for $q_0 = 0$, note they use $q_0 = 1$). If this absolute luminosity were entirely due to a power-law continuum, our observed value of W_λ (C IV, $z = 0$) = 33 Å would place 53W002 well outside the locus occupied by Seyfert galaxies or quasars in their Baldwin diagrams. If only ~35% of the continuum comes from the power law—and thus its W_λ(C IV, AGN) = 94 Å—then again 53W002 falls in the region of luminous Seyfert galaxies, close to low-luminosity QSOs as in the Kinney et al. diagrams.

3.7. *Classification of 53W002*

The rest-frame radio power of 53W002 is $\log P_{1.4} = 27.88$ W Hz^{-1}, which is ~3 dex higher than the *most* powerful nearby radio Seyferts (Windhorst 1984). If its present-day counterpart were indeed a Seyfert 1, this would imply a population evolution proportional to $(1 + z)^{5.5}$, as strong as for the most powerful radio quasars. A more likely cosmological evolution at these powers [$\propto(1 + z)^4$; Windhorst et al. 1990] would reduce its present-day radio power to $\log P_{1.4} \sim 25.76$ W Hz^{-1}. This is intermediate between the most powerful nearby radio Seyferts and low-power radio quasars. It is a typical radio power for nearby giant elliptical galaxies.

For this reason, we believe that the present-day counterpart of 53W002 is *not* necessarily a Seyfert [or a spiral, for which even more drastic evolution proportional to $(1 + z)^{9.5}$ would be required], but more likely a low-power radio quasar or *giant elliptical galaxy*. The fact that 53W002 has a Seyfert 1–like AGN at $z = 2.390$ thus does not necessarily mean that it is still a Seyfert galaxy at $z = 0$. The classification and evolution of 53W002 as an individual object thus cannot be understood without the perspective of the cosmological evolution of the *entire* radio galaxy and AGN population.

4. COMPARISON OF 53W002 AT $z = 2.390$ WITH NEARBY OBJECTS

Star-forming early-type galaxies such as NGC 5102, NGC 205, NGC 2681, and NGC 4742 provide examples of present-day stellar populations that have apparently undergone a recent dominant starburst (Burstein et al. 1988). They were able to estimate the ages of these bursts, providing a straightforward template against which the far-UV SEDs of high-redshift galaxies may be compared (Fig. 7). For NGC 5102, the starburst occurred about 0.3 Gyr ago. For NGC 2681, the amplitude of the UV continuum is substantially fainter, and its starburst is probably about 1–2 Gyr old. In both galaxies, the currently observed starburst dominates the *older* stellar population in the UV. Hence, these galaxies may have UV spectra that are the closest analogs to those of young galaxies. In the active galaxy M87 a rising UV upturn is noticeable below 1500 Å, which is a common feature of early-type galaxies.

In the rest of this paper, we will refer to "galaxy age" as the time that has passed since the *first major* starburst *started* which formed the bulk of stars we observe. That is, we will not be able to constrain the formation epoch of a much earlier starburst (e.g., Population III stars) involving only a few percent of the total galaxy mass that will eventually form stars.

4.1. *Internal Reddening*

Internal extinction by dust will little change the slope of the far-UV SED, since the relative extinction from 1800 Å varies by less than a factor of 1.6 (e.g., Seaton 1979). Relatively strong Lyα in 53W002 (from both the AGN and the starburst) also argues against significant dust absorption, since $A(1216\text{ Å}) \simeq 9 \times E(B-V) \simeq 3 \times A(V)$. If absorption longward of the 4000 Å break exceeded 0.1–0.2 mag, the extinction-corrected Lyα plus continuum flux would exceed that expected from a plausible AGN plus starburst, even if the central AGN were not more absorbed by the torus than the stellar continuum by the galaxy dust. In addition, high internal reddening would also be inconsistent with the SED of 53W002 (§§ 4.3 and 5).

All of the bright radio galaxies studied at high redshift have UV continua that turn down (in F_ν) below 1500–2000 Å (Chambers & McCarthy 1990). We do not believe that this is due to dust. None has a significant UV upturn, while this is seen in the spectra of a nonnegligible fraction of galaxy bulges at low redshift (Burstein et al. 1988; Keel & Windhorst 1991).

4.2. *Emission Lines*

4.2.1. *Comparison with Emission Lines of Nearby AGNs*

In the Kinney et al. (1991) *IUE* atlas, the Seyfert 1 galaxies 0531−002 and 1119+120 and the low-redshift QSOs 0026+129, 0121−590, 1229+204, and 2130+099 resemble 53W002 in its UV line ratios. These nearby AGNs have broader Lyα (usually blended with N v) and C IV wings than 53W002. Their broad-line components would be less pronounced if a *stronger* flat-spectrum stellar population was superposed as we suggested for 53W002. Comparing 53W002 with the broader line AGN discovered by Foltz et al. (1983) at $z = 2.47$, we arrive at the same conclusion: adding a stellar UV continuum of 2–3 times their AGN amplitude would make its spectrum look like 53W002.

A noticeable difference is that the observed N v/Lyα ratio in 53W002 is ~2 times stronger than the average value seen in most nearby AGNs (see also Kwan & Krolik 1981). The fact that nitrogen is seen 4 times ionized requires temperatures too high even for early O stars, and is thus most likely caused by the AGN continuum. One could test for the expected central concentration of N v (plus some reflected light from a cone) by imaging 53W002 on a large telescope with a special redshifted N v narrow-band filter that excludes all adjacent Lyα.

4.2.2. *Comparison with Emission Lines of Nearby Radio Galaxies*

The Lyα line of 53W002 is resolved, both spatially (Fig. 3) and spectrally (Fig. 4*b*). It has an observed FWHM of ~21 Å and a (Gaussian-) deconvolved velocity width of 1390 km s^{-1} (FWHM). With $\sigma_v \sim 590$ km s^{-1} and a rest-frame $(1559 - V)$ color of ~0.1 mag (§ 2.6), 53W002 falls somewhat outside the $(1550 - V)$ versus velocity dispersion diagram of Burstein et al. (1988). This sample of present day early-type galaxies has an average velocity dispersion of 215 km s^{-1}, increasing to 400 km s^{-1} for a massive galaxy like M87. The Lyα and C IV velocity width of 53W002 are somewhat too large for a completely virialized galaxy, and likely have contributions from its Seyfert 1–like central engine and a dynamically collapsing system.

Figure 4 gives the 12.5 hr rest-frame *IUE* spectrum of M87 (Buson et al. 1990). Its rest-frame Lyα equivalent width is $W_\lambda(z = 0) \sim 13$–66 Å (presumably closer to 66 Å, but hard to measure because of the strength of geocoronal Lyα). In comparison, we find W_λ(Lyα, $z = 0$) = 80 ± 25 Å for 53W002, or 154 Å when compared with the AGN continuum *alone* (§ 3.6). These W_λ(Lyα, $z = 0$) values are intermediate between the 20–70 Å range observed in nearby low-luminosity radio galaxies (Keel & Windhorst 1991) and the most powerful high-

redshift radio galaxies [whose W_λ(Lyα, $z = 0$) can be several hundred angstroms; § 5.3]. The likely starburst component of W_λ(Lyα, SB) $\simeq 26 \pm 10$ Å of 53W002 is similar to the range observed for low-redshift radio galaxies, indicating that its SFR cannot be as high as in the most powerful high-redshift radio galaxies. The composite UV spectrum of M87 (§ 4.4) implies that the ionizing flux to produce its Lyα emission must come from a combination of old and young hot stars, as well as perhaps from its LINER (Keel & Windhorst 1991). Thus, the fact that M87 and 53W002 have similar W_λ(Lyα) can be attributed more to the similarity of their total available ionizing flux than to the similarity of its physical origin.

4.3. *Limits to Possible UV Absorption Features*

Table 3 lists the wavelengths of possible UV absorption features of stellar or interstellar origin (Underhill, Leckrone, & West 1972; Panek & Savage 1976; Underhill 1982; Prinja 1990). Most of these are *not convincingly* detected in 53W002's spectrum, but their lack of detection can place limits to the age of its stellar population. The detection of several C, O, and Si UV absorption features with $W_\lambda \sim 2$–4 Å was reported in low-redshift starburst galaxies by Lamb et al. (1985), and for high-redshift actively star-forming radio galaxies by Chambers & McCarthy (1990).

The two "features" at 1426 Å (Si II) and 1478 Å (Si I + Si II) could be real in Figure 4*b*; they are also (barely) seen in the M87 spectrum (Fig. 4*c*). The 1426 Å feature survives in the smoothed spectra of both galaxies in Figure 7. *IUE* spectra have fixed pattern noise, which may be the explanation for the 1840 Å "feature" in M87's spectrum. This, as well as most other absorption-line candidates listed in Table 3 do not exceed the 1–1.5 σ level in 53W002. Section 4.2 suggested that most of 53W002's $\sim$ 600 km s^{-1} velocity dispersion is due to its AGN, with an expected contribution of $\sigma_v \simeq$ several 100 km s^{-1} from its stellar population. Figure 4*b* and Table 3 show that the corresponding 2–4 Å equivalent width expected for most stellar absorption features is indeed still beyond the limit of our MMT spectrum, which has an W_λ detection limit of $\sim$5 Å.

From the lack of detected absorption features, the following limits may be placed to the turnoff age of 53W002's current stellar population (ignoring the effect of the $\sim$35% nonthermal component on the absorption-line equivalent widths). The lines Si IV λ1399 and C II λ1335 cannot be used, since they are seen in emission in some high-redshift 3CR radio galaxies (McCarthy 1991). The observed absorption line W_λ versus spectral type relations (Panek & Savage 1976; Underhill 1982; Prinja 1990) suggest that 53W002's dominant spectral type is (1) later than B7.5 V from the lack of detected Si III λ1299 and (2) earlier than A9 V from the lack of detected Si II λ1265. If the main-sequence (MS) turnoff of 53W002 is in the range B7 V–A0 V, the strength of absorption features in Figure 4 should be minimal. Their detection will require higher resolution and higher signal-to-noise spectra, and place important limits to the nonthermal component.

4.4. *53W002's Continuum Compared with Nearby Stellar Populations*

For the study of stellar populations, it is irrelevant to what kind nearby galaxies we compare the high-redshift galaxies, *provided* that both have a *homogeneous and representative* stellar population within our photometric apertures, *and* that our library of present-day stellar populations brackets the age of the stellar population seen in 53W002. *IUE* spectra of nearby early-type galaxies with the *same* metallicity (Burstein et al. 1988) are *independent* of exposed linear size within a factor of 5–20, covering 0.1–5 kpc within similar UV and ground-based apertures.

Figure 7 compares 53W002's UV SED to the *IUE* spectra of NGC 5102, NGC 2681, and M87 (NGC 4486) in order of progressing star formation history. These nearby galaxy spectra are labeled with the most likely value for their current ages. The errors in normalizing the log $F_\lambda(1550)$ – log $F_\lambda(V)$ colors are $\sim$0.1 dex in each case (Burstein et al. 1988). Some of the drop in the 53W002's SED below Lyα might be caused by intervening absorbers, analogous to the Lyman forest in QSO spectra. The Lyman discontinuity could not be detected in 53W002, since it is right at the atmospheric cutoff ($\sim$3100 Å).

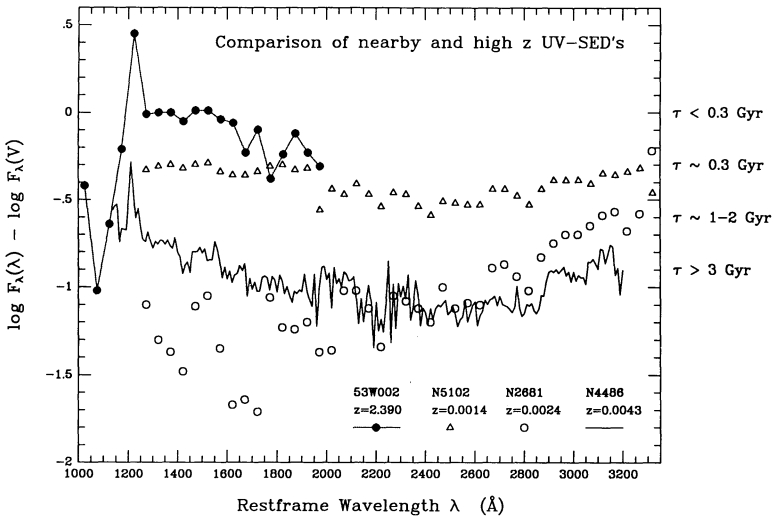

FIG. 7.—Comparison of rest-frame MMT spectrum of 53W002 (*filled circles + solid line*) and summed *IUE* exposures of several nearby early-type galaxies from Burstein et al. (1988): NGC 5102 (*triangles*) M87 (NGC 4486) (*solid line*); and NGC 2681 (*open circles*). Plotted are the log $F_\lambda(\lambda)$ – log $F_\lambda(V)$ flux vs. wavelength. The nearby galaxy spectra are labeled with age estimates from the amplitude and slope of the UV continuum (Burstein et al. 1988). The spectrum of 53W002 is more UV-luminous than that of any of the other galaxies, suggesting an upper limit to its age of $\sim 3 \times 10^8$ yr or less.

The M87 spectrum below Lyα is highly uncertain because of the saturated geocoronal line (§ 2.7).

M87 shows the well-known hot UV upturn below 1500 Å, which could be due to either ongoing star formation or a hot component of the old stellar population (e.g., Burstein et al. 1988; Bertelli, Chiosi, & Bertola 1989; Barbaro & Olivi 1989). It is unavoidable that hot, evolving post–asymptotic giant branch (PAGB) stars contribute at some level to the SEDs of old stellar populations in *present-day* galaxies. Comparison of M87's spectrum with that of more quiescent nearby early-type galaxies suggests that much of its far-UV continuum may come from the hot *old* stellar population, combined with an additional minority source of very recent star formation ($\lesssim$0.1 Gyr; Bertola 1988). This UV upturn is also seen in several nearby weak radio galaxies studied by Keel & Windhorst (1991). In contrast, at $z = 2.390$ the high-redshift galaxy 53W002 has not had enough time to build up a significant far-UV component from PAGB stars, which do not develop until the stellar population is older than about 3 Gyr.

It is important to compare *both* the *shape* of the far-UV SED *and* its *amplitude* [or (1550 − V) color] in the rest frame. A relatively flat far-UV SED is consistent with a high amount of recent star formation *if* the (1550 − V) color is very blue, but implies a relative absence of recent star formation if very red. Compared with the rest-frame V band, the UV continuum of 53W002 has a much higher amplitude than any of the nearby galaxies in Figure 7. It is even more UV-luminous than the starburst galaxy NGC 5102, which is the youngest stellar population in the Burstein et al. sample. The progressive decrease with age of the UV continuum amplitude limits the age of the currently observed starburst in 53W002 to $\sim$0.3 Gyr or less. The presence of the nonthermal power law could reduce the amplitude of 53W002's continuum downward by 0.2 dex in log $F_\lambda(1550)$ − log $F_\lambda(V)$, but it would still be more UV-luminous and thus younger than NGC 5102.

A similar estimate of the currently observed starburst age can be obtained from the *slope and shape* of 53W002's *UV spectrum alone.* One can compare Figure 7 directly with the late B-type LMC *supergiants* of Fitzpatrick (1987), which have slightly different log $F_\lambda(1550)$ − log $F_\lambda(V)$ normalization. This sequence of spectra shows that the MS turnoff stars in 53W002 have to be cooler than log $T_{\rm eff} \sim 4.03$ (later than B9 V; MS turnoff $\lesssim 3\ M_\odot$), or older than $\sim$0.25 Gyr.

In conclusion, this section gave three estimates for the MS turnoff age of the currently observed starburst in 53W002, each consistent with 0.25–0.3 Gyr. Since its star formation occurs over the *full* 67 × 40 kpc *size of the Ly*α *cloud*, all these data suggest that a global star formation event took place in 53W002 less than 0.3 Gyr before the epoch of observation at $z = 2.390$. A starburst of this age would have started in 53W002 at $z \sim 2.5$ (for $H_0 = 50$, $q_0 = 0.0$), or $z_f \sim 3.0$ (for $H_0 = 90$, $q_0 = 0.5$). For such a young age of the starburst, the corresponding redshift where it started is *largely independent of cosmology.*

5. COMPARISON OF 53W002 WITH OTHER HIGH-z RADIO GALAXIES

Figure 8 shows the log F_ν versus log λ spectrum of 53W002 as derived from Lyα *UBgriJHK* photometry. Since $\sim$20%–

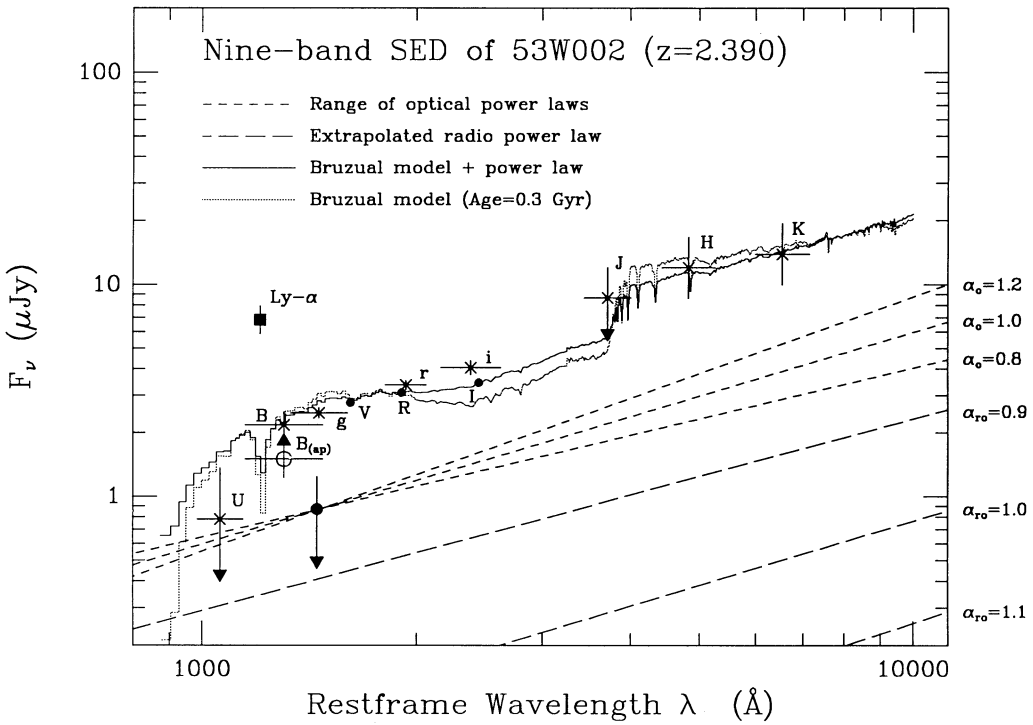

FIG. 8.—Rest-frame spectrum of 53W002 (in F_ν vs. λ) from calibrated nine-band photometry (Lyα *UBgriJHK*), all using total magnitudes with the same apertures and sky boxes (except for the extended Lyα). The open circle indicates a lower limit in Johnson B measured through the 2″ × 3″ MMT spectrograph aperture. The flux in U is possibly depressed by the Lyman forest. Long-dashed lines indicate power-law continua extrapolated from the rest-frame 1.412 GHz flux, labeled with the radio-optical spectral index (the observed *radio* spectrum itself has $\alpha \sim 1.2$). The short-dashed lines indicate the range of plausible nonthermal UV power-law continua [from the observed line ratios and $W_\lambda(z = 0)$], normalized at 1450 Å. The dotted line is a Bruzual spectral evolution model with age = 0.32 Gyr and no power law. The solid line has age = 0.25 Gyr and a power continuum with $\alpha = 1.2$ and $f_{1450}^{\rm AGN} = 35\%$. All models assume Salpeter IMF, and exponentially declining SFR with e-folding time $\tau = 0.1$ Gyr. The dominant component in 53W002's spectrum is presumably starlight with age $\lesssim$0.3 Gyr.

30% of the spectrophotometric flux may have been lost outside the MMT 2″ × 3″ aperture (§ 2.4), we compare the models of 53W002 to its broad-band colors (§ 2.6).

In interpreting 53W002's spectrum, one should keep in mind that the object is very faint in H and K, and that its J-magnitude is only an upper limit, whose interpretation depends on the shape of the J-filter, since it contains the redshifted 4000 Å break. At $z = 2.390$, the Palomar J-filter peaks at a rest-frame wavelength $\lambda = 3717$ Å, and extends from 3440 to 3995 Å. It thus mostly measures flux shortward of 4000 Å, and can constrain the 4000 Å break when compared with the H and K bands. Apart from a real measurement of stellar absorption features, an accurate measurement of the J-band flux would be the best evidence for a dominant stellar component in 53W002.

Given the modest equivalent width of starburst Lyα, we do not expect [O II] λ3727 to be strong enough to affect the flux in the wide J band by more than 10%. Similarly, although Hβ + [O III] and Hα are right in the middle of the wide H and K filters, respectively, they probably also do not effect these fluxes significantly.

5.1. *Effects of the Nonthermal Power Law*

The most likely power-law component of 53W002 (§ 3.6) is plotted in Figure 8 as short-dashed lines for $f_{1450}^{\rm AGN} = 35\% \pm 15\%$ and $\alpha = 0.8$, 1.0, and 1.2 (the likely α-range observed by Kinney et al. 1985). The long-dashed lines indicate an extrapolation of the *radio* power-law component (whose GHz spectral index $\langle a \rangle \simeq 1.2$; § 2.2) plotted for *radio-optical* spectral indices $\alpha_{\rm ro} = 1.1$, 1.0, and 0.9. Overall radio-optical power laws with $\alpha_{\rm ro} < 0.76$ are not allowed, since they would exceed the rest-frame UV flux of 53W002 in at least least one of the *observed* optical bands. A nonthermal continuum fraction $f_{1450}^{\rm AGN} = 35\%$ (§ 3.6) implies $\alpha_{\rm ro} \sim 0.85$, which is still consistent with the $\alpha_{\rm ro}$ distribution of Kron et al. (1985), who found that $\langle \alpha_{\rm ro} \rangle = 0.45$ with $\sigma = 0.17$ for 171 LBDS radio galaxies and quasars of similar radio fluxes (the fact that 53W002's UV flux is a combination of stellar and nonthermal flux somewhat complicates this argument).

A single *UV-optical* power law with slope $\alpha = 1.2$ could fit the entire broad-band spectrum (1200 Å $< \lambda <$ 7100 Å) in Figure 8, assuming that the U-band flux is depressed because of the intervening Lyman forest. However, a plot of the rest-frame F_ν versus ν spectrum shows that a *single* power law does *not* provide a good fit in the 1200 Å $< \lambda <$ 2000 Å range, because the MMT spectrum clearly turns down below 1500 Å. The broad-band optical data *alone* are actually good enough to constrain the slope of a power-law fit in the 1200 Å $< \lambda <$ 2600 Å range to $\alpha = 1.0$, which—when extrapolated to $\lambda > 3000$ Å—is about 0.15 dex lower than *all three* IR array points. This by itself does not exclude the possibility that the broad-band spectrum is dominated by a power-law component, but it shows that 53W002 could have a red bump with $D_{4000} \lesssim 0.13$ dex.

Let us now summarize the evidence against a dominant ($f_{1450}^{\rm AGN} \gtrsim 50\%$) nonthermal component:

1. The optical continuum is slightly extended and larger than the nonthermal radio source (§ 3.2). This does not necessarily mean that the optical continuum is starlight, because a nonthermal source could be beamed in the plane of the sky and then secattered toward us, so that its size only samples the reflecting medium, which can be much larger than the radio size.

2. The radio and optical continuum is nonvariable on time scales of years (§ 3.4). This argues against a dominant nonthermal contribution *only* if the nucleus is *not* obscured. Otherwise, the extended continuum may be reflected QSO light (Barthel 1989; Fabian 1989), and variability would be washed out because each seeing element samples $\sim 10^5$ yr of the QSO's history.

3. The observed Lyα line has a narrow-line component. The broad-line AGN component has the larger equivalent width, but is buried in a continuum that comes primarily from the starburst (see the line ratios in § 3.6). Since most of the Lyα flux comes from the nuclear region (§ 3.2), the fraction of Lyα flux ionized by the QSO cone must be small. Such a component could be broadened by reflection from a 10^7 K electron gas (Fabian 1989), but this is difficult to reconcile with the observed downturn in spectrum below 1500–2000 Å. Higher spectral and spatial resolution is required to determine accurately what fraction of the extended hydrogen gas is ionized locally by stars, or by a cone from the buried nucleus.

4. A single power law does not provide a good fit to the rest-frame MMT spectrum (F_ν versus ν) in the 1200 Å $< \lambda <$ 2000 Å range, because the spectrum turns down below 1500 Å (Fig. 8). Another way of stating this is that the spectrum shows some evidence for a modest 4000 Å break.

5. The UV spectrum may have a few (inter)stellar absorption features in common with nearby stellar populations and some high-redshift radio galaxies (§ .3).

6. Since 53W002 is a moderately powerful radio source, it is likely to develop an optical luminosity brighter than L^* (the break in the optical luminosity function) and therefore have a minimum stellar luminosity of at least a *few* times 10^{10} to 10^{11} $L_\odot$. Section 5.4 shows that a UV spectrum dominated by the nonthermal power law (i.e., $f_{1450}^{\rm AGN} \gg 50\%$) can harbor much less than 10^{11} $L_\odot$ in its remaining light. In other words, it is hard to hide an L^* galaxy underneath the power-law continuum if it is undergoing significant star formation at the time of observation. (If the power-law continuum had $\alpha \lesssim 0.8$, it could account for most of the UV continuum, and one would need a smaller [$\lesssim$a few times 10^{10} $M_\odot$] but older stellar population to explain the red bump.)

The first two arguments are model-dependent and can only be resolved by higher spatial resolution observations. We believe that these six arguments together form sufficient evidence against a majority nonthermal contribution. We will therefore consider two kinds of models: (*a*) no UV power-law continuum at all and (*b*) power laws with $f_{1450}^{\rm AGN} = 35\%$–$50\%$ and the likely range of slopes $\alpha = 0.8$–1.2, bearing in mind that any upper limits to 53W002's stellar mass will be more interesting if $f_{1450}^{\rm AGN} \gg 50\%$ or $\alpha > 1.2$.

5.2. *Comparison of 53W002 with Powerful Radio Galaxies at $z = 2$–3.8*

Here we compare 53W002 at $z = 2.390$ with the much more powerful high-redshift radio galaxies currently known from the 1 Jy survey at $z = 3.395$ (0904+34; Lilly 1988) and the 4C survey at $z = 2.3$–3.8 (Chambers et al. 1988, 1990, including 4C 41.17 at $z = 3.8$), as well as radio galaxies with $z \gtrsim 2$ from the Molonglo survey (McCarthy et al. 1990a).

If the light in 53W002 is indeed dominated by starlight, two pieces of evidence suggest that its SFR was higher in the immediate past (assuming a reasonable initial mass function [IMF]): its UV continuum and its small 4000 Å break.

5.2.1. *The UV Continuum*

The optical and optical-IR colors of 53W002 (Table 4) are very blue, and are consistent with model predictions from a young ($\lesssim 1$ Gyr) stellar population at $z = 2.4$ (see Fig. 7 of Windhorst 1986). According to Lilly (1988), 0902+34 has a much redder ($1550 - V$) color ($\sim +1.2$) at $z = 3.395$, implying that its star formation took place about 1–2 Gyr before it was observed at $z = 3.4$ (the "old" model in Table 5). However, a more recent measurement of 0902+34 (Lilly 1991) shows that its real K-band flux is at least 0.5 mag fainter, thereby reducing its age to 0.5–1 Gyr (the "young" model in Table 5). The galaxy of Chambers et al. (1990) at $z = 3.800$ has a similar (but brighter) UV continuum as 53W002, and somewhat redder ($1550 - V$) colors, consistent with a somewhat older stellar population but at a much earlier cosmic epoch. Both 53W002 and 4C 41.17 are still bluer than the corrected colors of 0902+34.

The UV spectrum of 53W002 *clearly turns down below* 2000 Å (Fig. 8), similar to that seen in other recently studied high-redshift galaxies (Chambers & McCarthy 1990). Without a nonthermal power-law component, this downturn corresponds to $\log T_{\rm eff} \sim 4.0$, or a 3 $M_\odot$ turnoff mass (age $\gtrsim 0.25$ Gyr). The *continuous* presence of stars younger than B9 V would be required to keep the UV continuum flat all the way down to the Lyα limit. For a reasonable IMF, the downturn in 53W002's spectrum thus indicates that its SFR must have been much higher in the immediate past. The "young" models in Table 5 describe that we are seeing the tail end of this star formation maximum after a few e-folding times of 10^8 yr.

5.2.2. *The* 4000 Å *Break*

The IR photometry indicates that 53W002 may have a red bump, among the weakest observed in high-redshift radio galaxies (Lilly 1988; Chambers & Charlot 1990; Chambers et al. 1990). The 4000 Å break is a measure of the ratio of past to present star formation. If the current starburst comprised the first generation of stars in 53W002, its spectrum would be roughly *flat* in F_ν with little or no 4000 Å break. Since 53W002 does have a small red bump, its SFR must have been (somewhat) higher in the past to produce the downturn in the UV continuum (§ 5.2.1).

The crucial question is *how* the SFR declined with time. Lilly (1989) suggested that the bulk of star formation in 0902+34 occurred at a much earlier epoch and was unrelated to the current starburst. Chambers & McCarthy (1990) and Chambers & Charlot (1990) pointed out that—given a Scalo or Salpeter IMF—the monotonically decreasing SFR required to fit the observed UV downturn also produces sufficient light longward of 4000 Å within the time scale of the *current* burst.

The small magnitude of 53W002's 4000 Å break suggests that its current starburst is certainly a major episode in the lifetime of the object, if not *the* major star-forming episode. The red bump in 53W002 is less than $D_{4000} \lesssim 0.13$ dex (§ 5.1), or a factor of ~ 1.3. This is at the *low* end of the observed range of 4000 Å breaks in high-redshift cluster galaxies (Dressler & Gunn 1990), and reflects a MS turnoff earlier than $\sim$A0 V (Bruzual 1983), consistent with our previous age estimates. Any previous starburst will be older than the current one, and must involve substantially fewer stars than the current burst comprises.

5.3. *Order-of-Magnitude Parameter Estimates*

Table 5 lists order-of-magnitude estimates for the relevant physical parameters of 53W002, 0902+34, and 4C 41.17. Sufficiently detailed data were not available to compute all parameters for other published radio galaxies at $z \gtrsim 2$. Most of these quantities are uncertain by at least 0.3 dex, and serve as illumination of the possible parameter range only. In particular, realistic values will depend on peculiarities of the IMF and SFR at $z \gtrsim 2.4$, which we discuss further in § 5.4.

Column (4) of Table 5 lists the SFR derived from the part of W_λ(Lyα) that is likely unrelated to the AGN. The small W_λ(C IV, $z = 0$) values in 0902+34 and 4C 41.17 show that their fractional AGN contribution to W_λ(Lyα) is probably less than in 53W002. This appears to be true also for most MC radio galaxies of McCarthy et al. (1990a, b). The first line of column (6) lists the best-fit turnoff ages, and the second line lists the corresponding redshift ("$z_{\rm form}$") when that starburst started. The total mass of *currently* luminous stars is listed in column (7) as SFR × t, where t is the turnoff age (the instantaneous SFR × t is smaller than the *total* mass processed into stars thus far, because the latter is integrated over an *exponentially decreasing* SFR which was higher in the past; § 5.2.1). Column (8) lists the distance modulus, and column (9) the K-correction in the V and K bands, respectively (from Bruzual 1983, 1988). At times this close to the starburst, K-corrections in V are actually *smaller* than in the K-band (contrary to common belief, the K-correction in the K bond is *only* smaller than in V at low redshifts). However, the K-corrections in the K band *are* less uncertain than those in V, the latter depending more crucially (~ 0.5 mag) on the precise observed age and decline of the SFR. The purpose of Table 5 is to demonstrate the *relative* values of the physical quantities, which are to first order similarly affected by these uncertainties.

Column (10) then lists the absolute magnitude in V and K, reduced to $z = 0$. Column (11) gives the estimated absolute V-luminosity for stars at the MS turnoff, and the second line gives the K-luminosity of the corresponding *coeval* stars at the red plus asymptotic giant branches. As the relative importance of the RGB and AGB also depends on the age of the starburst (Wyse 1985), a running time average over these absolute K-magnitudes was used.

The last column in Table 5 then gives the total galaxy mass *observed* as stars around the MS turnoff (from the V band) and at the RGB+AGB (from the K band), respectively. This follows as the product of the turnoff mass in column (5) and the number of stars implied by columns (10) and (11) assuming no internal extinction (see § 4.1). The fractional galaxy mass that radiates at—or just past—the MS turnoff is listed below the total mass (second line in col. [7]).

The continuum-subtracted Lyα flux, (Lyα − cont), of 0902+34 at $z = 3.395$ is 73 μJy, with corresponding luminosity L(Lyα) = 9.1×10^{37} W. For 4C 41.17, F_ν(Lyα − cont) = 75 μJy at $z = 3.800$ and L(Lyα) = 1.2×10^{38} W. The corresponding SFRs are 900–1200 $M_\odot$ yr^{-1} (Cohen & Smith 1990). For 53W002, F_ν(Lyα − cont) = 21 μJy and L(Lyα) = 9.7×10^{36}W. If all Lyα flux in 53W002 came from photoionization by hot stars, this implies SFR $\sim$ 100–300 $M_\odot$ yr^{-1}. Since about one-third (=26 Å/80 Å) of the observed Lyα flux comes from stars (§ 3.6), the corresponding SFR is $\sim$30–100 $M_\odot$ yr^{-1}, much lower than in the other high-redshift radio galaxies. We adopt the value of 100 $M_\odot$ yr^{-1} for 53W002. In these estimates, we assume that the *physics* of star formation regions—which explains the relationship between L(Lyα) and the SFR—does not vary among radio galaxies, or with cosmic epoch.

5.4. *Comparison of 53W002 with Specific Models*

Our models used the Bruzual (1983, 1989) evolutionary synthesis code, as modified by Chambers et al. (1990) to include smaller times steps. All stellar evolution tracks are for solar

TABLE 5

COMPARISON OF PHYSICAL PROPERTIES OF 53W002 WITH OTHER HIGH-z RADIO GALAXIES

Object (model) (1)	z_{obs} (2)	W_λ ($z=0$) (Å) (3)	⟨SFR⟩ $M_\odot$ yr^{-1} (4)	M_{to}/Sp Sp(pms) ($M_\odot$) (5)	Age z_{form} (Gyr) (6)	M_{tot} (%) ($M_\odot$) (7)	D_{mod} (mag) (8)	$K_V(z)$ $K_K(z)$ (mag) (9)	M_V M_K (mag) (10)	M_V^{to} M_K^{pms} (mag) (11)	M_{to}^* M_{pms}^* ($M_\odot$) (12)
53W002(young)	2.390	80 ± 25	~300 ± 100	2.7/A0 V	0.32	1E11	47.48	−0.5	−24.2	−0.0	1.3E10
				K3 III	2.59	19%		−1.7	−26.6	−3.3	5.6E09
53W002, $+\alpha = 1.2$	2.390	26 ± 10	~100 ± 50	3.0/B9 V	0.25	3E10	47.48	−0.6	−23.6	−0.6	4.8E09
				K2 III	2.55	42%		−1.7	−26.1	−2.9	5.6E09
53W002, $+\alpha = 1.0$	2.390	26 ± 10	~100 ± 50	2.7/A0 V	0.32	3E10	47.48	−0.5	−23.7	−0.0	8.4E09
				K3 III	2.59	39%		−1.7	−26.2	−3.3	4.0E09
53W002, $+\alpha = 0.8$	2.390	26 ± 10	~100 ± 50	2.5/A1 V	0.40	4E10	47.48	−0.4	−23.8	+0.2	1.0E10
				K4 III	2.64	31%		−1.7	−26.3	−4.0	2.1E09
0902+34 (young)	3.395	300 ± 50	>700 ± 300	1.7/A4 V	$\lesssim$1.0	7E11	48.69	−0.4	−25.8	+2.0	2.2E11
				K7 III	4.7	33%		−1.7	−28.0	−4.4	4.7E09
0902+34 (old)	3.395	300 ± 50	>700 ± 300	1.5/A7 V	1.5	1E12	48.69	−0.0	−26.2	+2.4	4.1E11
				M0 III	>5.5	39%		−1.6	−28.6	−5.5	2.6E09
4C 41.17 (young)	3.800	390 ± 50	~1200 ± 600	2.5/A1 V	0.4	5E11	49.10	−0.4	−26.7	+0.2	1.4E11
				K4 III	4.3	34%		−1.7	−28.7	−4.0	1.9E10
4C 41.17 (old)	3.800	240 ± 40	~700 ± 300	1.5/A7 V	1.5	1E12	49.10	−0.0	−27.1	+2.4	9.4E11
				M0 III	>6.5	90%		−1.6	−28.8	−5.5	3.1E09

Col. (1).—First model for 53W002 does not include nonthermal power-law component. The other models assume $f_{1450}^{AGN} = 35\% \pm 15\%$ and are described in the text. The young model of 0902+34 is based on its revised K-magnitude (~19.0; Lilly 1991).

Col. (3).—Starburst-related rest-frame W_λ(Lyα, $z = 0$) and its error.

Col. (4).—Average star formation rate ⟨SFR⟩ (in $M_\odot$ yr^{-1}) and estimated error.

Col. (5).—M_{to}(Sp) = best-fit turnoff mass and spectral type. Second line gives Sp(pms) = corresponding spectral type of dominant stellar luminosity on post–main sequence (RGB+AGB).

Col. (6).—Age corresponding to M_{to} in Gyr. Second line lists z_{form} = redshift at which corresponding stars started forming (for $H_0 = 50$ km s^{-1} Mpc^{-1}, $q_0 = 0$).

Col. (7).—M_{tot} = total mass processed into stars (in $M_\odot$) ≃ ⟨SFR⟩ × age. Percentage in the second row indicates what fraction of the total mass is at the turnoff point plus the post–main sequence (see col. [12]).

Col. (8).—Distance modulus for $H_0 = 50$, $q_0 = 0$.

Col. (9).—$K_V(z)$, $K_K(z)$ = estimated K-correction for starburst of age t observed at z_{obs}, in V and K bands, respectively.

Col. (10).—M_V, M_K = total absolute magnitude in V and K reduced to $z = 0$.

Col. (11).—M_V^{to} = absolute V-magnitude of stars at main-sequence turnoff; M_K^{pms} = absolute K-magnitude of corresponding *coeval* stars at post–main sequence.

Col. (12).—M_{to}^* = corresponding galaxy mass at main-sequence turnoff; M_{pms}^* = corresponding mass at AGB+RGB.

metallicity only, which is justified in § 6.1. The models are computed with a Scalo (1986) IMF with lower and upper mass cutoffs of 0.08 and 75 $M_\odot$, respectively. Models with a Salpeter IMF give similar results, except very shortly after the starburst, where the most massive stars do make a difference. In our models, the SFR declines exponentially with an e-folding time $\tau = 1.0 \times 10^8$ yr, so after the first 0.2 Gyr the (uncertain) high end of the IMF should no longer matter.

In Figure 8 we compare two synthetic model spectra with the rest-frame broad-band colors of 53W002. The dotted line is a stellar population model *without* power-law contribution. Its age at $z = 2.390$ is 3.2×10^8 yr. Our models show that the *total* mass of 53W002 processed into stars is $\sim 4 \times 10^{11}$ $M_\odot$ for $q_0 = 0$, or 2×10^{11} for $q_0 = 0.5$ (as explained in § 5.3, this mass is larger than the values in Table 5, which were estimated from stars radiating around—and just past—the MS turnoff). The *current* SFR of 53W002 in our models is 100 $M_\odot$ yr^{-1} or less. Our model also predicts the number of Lyman continuum photons from the stellar population. If each ionizing photon produces a Lyα photon, the W_λ(Lyα, $z = 0$) value due to the stellar population would be 40–75 Å. The higher number does not account for absorption at 1216 Å in stellar photospheres. The lower number includes the expected destruction of Lyα photons (Fig. 8), and is in agreement with the starburst-related value of W_λ(Lyα, $z = 0$) = 26 ± 10 Å derived in § 3.6.

The solid line in Figure 8 is a similar stellar population with $f_{1450}^{AGN} \sim 35\%$ and an $\alpha = +1.2$ power law added. A best fit yields a marginally younger spectrum with age 2.5×10^8 yr. These ages could be a bit younger by assuming $\tau = 5 \times 10^8$, but $\tau = 10^8$ yr is more consistent with the other high-redshift radio galaxies. It is hard to make 53W002 much younger than 0.2 Gyr without making the IMF substantially flatter.

The alternative model—an old plus a young burst—does not fit the far-UV spectrum. One could, however, hide an older population of much lower mass ($L \ll L^*$) underneath the presently observed spectrum, and argue that the blue light is just a few percent of the galaxy mass involved in the currently observed starburst. This is Lilly's (1988) explanation for 0902+34. We believe that this model disagrees with 53W002's UV spectrum, which indicates that a much larger fraction of its luminous mass must be involved in the present starburst, the tail end of which we observe. The age of 53W002's current starburst may be related to the typical time scale for a radio source to start playing a dominant role [~(1–2) × 10^8 yr].

5.5. *Results*

The exciting aspect of 53W002 is that its luminous mass is *only* that of an L^* galaxy at best. The most powerful 3C, 4C, and 1 Jy radio galaxies at similar or higher redshifts have extremely low space density and masses of ~5–8 L^* (depending on cosmology). These are thus rather unusual objects. If 53W002 has—or will develop into—an L^*-like mass, it may indeed be the progenitor of a *normal* early-type galaxy, or possibly a massive spiral or a Seyfert. Since its radio power is ~3 dex higher than the most powerful radio Seyferts (§ 3.7), it

is more likely that the 53W002 will develop into a present-day giant elliptical galaxy or a low power radio quasar.

With the additional ~35% power-law contribution in 53W002, it will be very hard to hide earlier massive starbursts longward of the 4000 Å break. Table 5 shows that 53W002 does not have an absolute magnitude luminous enough to hide those stars, unless our observed IR fluxes were grossly underestimated, or the currently observed starburst does not radiate longward of 4000 Å, or the young galaxy has substantial internal absorption (unlikely for standard extinction; § 4.1).

We emphasize that these models are limited by fundamental unknowns such as the IMF, the SFR, the nonthermal power-law component, etc. We believe that the most plausible models for each of the galaxies in Table 5 are the young ones (in the case of 53W002 with a 35% power-law continuum). In all three young models about 30%–40% of the *total* mass currently involved in the starburst is seen around the MS turnoff. This is expected for a normal IMF, and suggests that the model for 53W002 *without* nonthermal component (where this fraction is only 19%) and especially the old model for 4C 41.17 (with 90%) are not likely valid without invoking a contrived IMF.

Since the broad-band photometry points in Figure 8 are close to a power law with slope $\alpha = 1.2$, increasing the power-law component to $f_{1450}^{\rm AGN} > 50\%$ does not make 53W002 much younger. The nonthermal continuum would add both to the red bump and the UV continuum, and would only reduce the total amount of light available for stars. A flatter power law ($\alpha \lesssim 0.8$) would increase the age somewhat, but this would be flatter than most of the UV power-law continua observed by Kinney et al. (1985). With a steeper ($\alpha > 1.2$) power law, the nonthermal contribution in the rest-frame visual could exceed 50% and the slope of the remaining stellar contiuum would be flatter, roughly corresponding to a MS turnoff of B6–7.5—or ~4–5 $M_\odot$—and inconsistent with the independent age estimates from § 4. Given that Kinney et al. (1985) find that some AGNs have power-law spectral indices steeper than $\alpha = 1.4$, it is possible that 53W002's power-law contribution in the rest-frame far-red is larger than our assumed value of 35%–50% (Fig. 8). If this nonthermal contribution is seen in reflection—and thus spatially extended—it may explain some of the uncertain growth curve in the K band noted in § 3.2. In that case, the limits to the stellar mass in 53W002 would be even more stringent if $f_{1450}^{\rm AGN} > 50\%$, which is our main objection against 53W002's UV spectrum being primarily a nonthermal power law. We do believe that quasars reside in galaxies, and that galaxies consist of stars. Table 5 shows that the integrated *stellar* luminosity can match or exceed that of AGNs during and shortly after a massive initial starburst—except for the most luminous high-redshift QSOs (§ 6.5).

6. SUMMARY AND DISCUSSIONS

Our discussion centered around the multiwavelength observations of a weak radio galaxy—53W002—from the Leiden Berkeley Deep Survey discovered at a redshift of 2.390. Our findings are summarized as follows:

1. The wavelength-dependent optical continuum morphology of 53W002 is quite compact (~10–35 kpc for $H_0 = 50$, $q_0 = 0$). In redshifted Lyα, the galaxy is more extended ($\lesssim$67 kpc × 40 kpc), but not as large as the most powerful high-redshift radio galaxies (§ 3.2).

2. The steep-spectrum radio source 53W002 is very *compact* (LAS ~ 0.″7 at 0.″15 resolution), ~2 times smaller than the UV-optical continuum and ~7 times smaller than the Lyα cloud. Image deconvolution shows that the radio source is aligned with both the extended Lyα image *and* the best-seeing optical continuum images (ΔP.A. $\lesssim 10°$). The suggested mechanism for the extended Lyα emission—jet-induced star formation combined with scattered radiation from a hidden quasar—may therefore be more widespread than previously thought (§ 3.3).

3. Nine-band photometry (Lyα *UBgriJHK*) shows one surrounding galaxy with a compact core that is variable on time scales of years. The source 53W002 itself is not variable, either in the radio or in the optical (§ 3.4). Only one other neighboring galaxy shows some excess light at 4100 Å, and may be at the same redshift (§ 3.5).

4. The source 53W002 has relatively weak and narrow Lyα (rest-frame $W_\lambda \sim 80$ Å), and relatively strong and somewhat broader N v and C iv, indicating a Seyfert 1–like AGN (§ 4.2). Comparison of its UV line ratio to those of AGNs constrains the *nonthermal power law* to 35% ± 15% of the *observed UV continuum* at 1450 Å (§ 3.6). Section 5.1 summarizes six arguments against a dominant nonthermal power-law contribution in 53W002's UV spectrum.

5. We compared the rest-frame UV-optical spectrum of 53W002 with *IUE* spectra and UV-optical colors of (*a*) present-day early-type galaxies; (*b*) actively star-forming galaxies; (*c*) low-power radio galaxies; (*d*) Seyferts; and (*e*) QSOs. Four independent age estimates yield consistent values of 0.25–0.32 Gyr, a MS turnoff in the range B9 V–A0 V, or 3–2 $M_\odot$ (§§ 4.3, 4.4, 5.2.2, 5.4).

6. We also compared 53W002 with other powerful high-redshift radio galaxies at $z = 2$–3.8 from the bright radio surveys. These other objects have much stronger Lyα and weaker C iv (smaller $f_{1450}^{\rm AGN}$), while 53W002 has much weaker W_λ(Lyα) and—after subtracting its nonnegligible AGN component—about a 10 times lower SFR ($\lesssim 100\ M_\odot\ {\rm yr}^{-1}$). Its age estimates, SFR, *and* observed absolute luminosities M_V and M_K are consistent with a *maximum* mass processed into stars of a *few* times $10^{11}\ M_\odot$ at $z = 2.390$.

6.1. *The First Major Starburst in 53W002?*

From the models discussed in § 5, and the order-of-magnitude estimates in Table 5, we can now draw the main conclusion in this paper: For reasonable parameters of the ionization and SFR in 53W002, this galaxy is currently undergoing one of *its major starbursts*, and has at $z = 2.390$ a much smaller *luminous* mass—at most a *few* times $10^{11}\ M_\odot$—than the more powerful steep-spectrum radio galaxies at $z = 2$–3.8.

This conclusion is based on a twofold argument: 53W002 has reduced absolute magnitudes that are *at least* 2.0–2.5 mag *fainter* than these most powerful radio galaxies at higher redshifts, and its starburst is younger. In addition to the ~10 times weaker Lyα flux from the starburst, this shows that *53W002 did not form stars as quickly, did not form as many stars, and did not start to form stars as early on as the more powerful radio galaxies at* $z = 2$–3.8.

In order to account for the observed 4000 Å break in 53W002, the SFR in this galaxy was probably higher in the past (1–3) × 10^8 yr. It is difficult to hide an earlier—and hence older starburst by the blue continuum of the currently observed starburst, especially because of its nonnegligible power-law contribution. Given the uncertainties in the SFR, the IMF, and the nonthermal contribution, and earlier star

formation epoch involving substantially less mass cannot be ruled out.

We are left with the tantilizing possibility that 53W002 does not have a major red bump, and is a genuinely young galaxy—with a weak AGN—that is seen during its first major starburst which started 0.3 Gyr before $z = 2.390$. With at most a few times $10^{11}\ M_\odot$ in luminous mass, 53W002 can hardly be called a massive stellar system at the top of the optical luminosity function. If 53W002 were to develop into what we believe are the present-day counterparts of high-redshift intermediate-power radio galaxies—massive early-type galaxies—it will need to form at least another $\sim 5 \times 10^{11}\ M_\odot$ in stars, which at this rate would take several more Gyr.

The high abundance implied by the presence of N v and C iv in its AGN (§ 4.2.1) does not mean that 53W002 has to be relatively old. The massive O- and early B-type stars that produce the required supernovae evolve on time scales of a *few* times 10^6–10^7 yr. If they enrich the interstellar medium in a few duty cycles, 53W002 can reach solar abundance within $\sim 10^8$ yr. Keel & Windhorst (1991) suggested that the stronger Lyα in high-redshift radio galaxies (of comparable radio power) may be in part due to a smaller dust content. If so, this illustrates that the chemical evolution in these galaxies has just started, and perhaps not yet completely reached solar abundance. Our models do not (yet) take chemical evolution into account, and assume that the stellar population achieve solar-like abundances well within the first e-folding time of the models ($\tau = 10^8$ yr).

6.2. *The Epoch(s) of (Radio) Galaxy Formation*

Our study indicates that the epoch of first major star formation in 53W002 did not appear to start until $z_{\rm form} = 2.5$–3.0 (for any cosmology with $H_0 = 50$–100 and $q_0 = 0.0$–0.5), or at $z_{\rm form} \sim 2.7$ for cosmologies (barely) consistent with the globular cluster ages (both for $H_0 = 50$ and $q_0 = 0.5$ *and* for $H_0 = 90$ and $q_0 = 0.0$). The "formation" epoch of 53W002 is thus considerably later than that of the highest redshift powerful radio galaxies, which have $z_{\rm form} \gtrsim 4$–7 (Table 5). This is a crucial point, because 53W002 is drawn from a sample of $\sim 10^5$–10^6 sources sr^{-1}, compared with $\sim 10^2$ sources sr^{-1} at brighter radio fluxes. It may be encouraging for the CDM theory of galaxy formation that at least this one L^*-like object did not appear to start forming stars much before $z \sim 2.5$–3.0.

The apparently wide range of (radio) galaxy ages at a given redshift suggests that these objects do not necessarily form the bulk of their stars coevally, but *start* doing so over a wide range of cosmic time. This is consistent with models for the epoch-dependent radio luminosity function which are constrained by radio source counts and redshift distributions (Windhorst 1984; Oort 1987; Condon 1989). These models suggest that the *most* powerful radio sources have higher values for the redshift cutoff than the less powerful ones (the 95% value of $z_{\rm max}$ ranges from 1 to 2.5 in these models). The epoch of radio galaxy formation—where galaxies first turned on their radio sources and underwent their first major starburst—could thus be a function of galaxy mass, in that the most luminous and rarest systems formed first. Although the numerical value of these redshift cutoffs may have been underestimated in some models, the point remains that a *single large* value of the redshift cutoff—and $z_{\rm form}$ as argued in this paper—is hard to reconcile with the available survey data. It is therefore important to study complete samples of weak radio sources spectroscopically, and see whether most P^*-like radio galaxies (with absolute magnitudes $\sim L^*$) started forming their stars at considerably later cosmic epochs than the most powerful ones.

6.3. *The "Alignment Effect" as a Function of Radio Power*

If the aligned continuum component of 53W002 is truly larger than the physical extent of the radio source, this may be due to nonthermal emission scattered into our line of sight and thus should be strongly polarized (Barthel 1989; Fabian 1989; di Sergo Alighieri et al. 1989; Scarrot, Rolph, & Tadhunter 1990). Some of the extended Lyα emission may be due to anisotropic ionizing radiation from the hidden quasar, as expected in Barthel's (1989) unification model. This is the explanation for many powerful high-redshift radio galaxies (Chambers et al. 1990; McCarthy et al. 1990a). In this model, the origin of the alignment is a combination of the hidden quasar light and jet-included star formation. Both a collapsing and an aging stellar population, as well as scattered light from the AGN, would result in (deconvolved) image sizes that increase toward shorter wavelengths (§ 3.2).

6.4. *Are Optically Fainter Radio Galaxies Necessarily at Larger Redshifts?*

The fact that we can observe a galaxy like 53W002 at $z = 2.390$ with $V \sim 23$ mag is of course due to the *high amplitude* of its UV continuum (compared with rest-frame V). Figure 7 shows that other galaxies can be easily 3–4 mag fainter in their rest-frame UV. If they were at the same redshift, they could be as faint as $V \sim 26$–27 mag, consistent with the magnitude distribution of weak radio source samples which are nearly 100% completely optically identified down to $V \simeq 27$ mag (Windhorst et al. 1987; Fomalont et al. 1991). Radio galaxies with $V \simeq 26$ mag are not necessarily at $z > 3.5$ as Heisler & Ostriker's (1988) dust obscuration model implies, but could be simply dormant galaxies like NGC 2681 that formed their stars 1–2 Gyr before we observed them at $z = 1.5$–3. Since high-redshift *radio* galaxies may have higher UV amplitudes than high-redshift quiescent galaxies, complete redshift samples will be required to check this possibility. This is an important challenge to the next generation of telescopes.

6.5. *Consequences for the Baldwin Effect*

Our studies show that an apparently young galaxy like 53W002 may have both significant contributions from its stellar population *and* a nonthermal UV continuum (the latter may either come directly from the QSO, or be seen in reflection). Depending on the exact (time evolution of the) value of $f_{1450}^{\rm AGN}$, a young galaxy can largely hide as an AGN, *or* may *dominate* the UV spectrum of an apparent AGN for some time. This may have consequences for studies that involve the *continuum* of QSOs, such as the Baldwin effect (as summarized by, e.g., Wampler et al. 1984; Baldwin et al. 1989). Table 5 suggests that a young galaxy at $z \gtrsim 2.5$ may have absolute UV magnitudes in the range $M_{1450} \sim -22.5$ to -25.5 ($H_0 = 50$, $q_0 = 0$). Since young galaxies are expected also to have a flat spectrum ($\alpha \lesssim 1$), their stellar population may contribute significantly to the "quasar" continuum, hence affecting the *determined* values of $W_\lambda(z = 0)$—given its definition in terms of *total* continuum flux—except for the most luminous QSOs. Projection effects in the unification model (Barthel 1989) may also increase the observed values of $W_\lambda(z = 0)$ toward fainter QSO luminosities (hence explaining the Baldwin effect), since most of their UV flux is scattered away in the torus, which is

why they appear as weaker AGNs. Hence, the observed W_λ increases toward lower AGN luminosities, not because the line is necessarily more luminous but because the quasar UV continuum is depressed with respect to the young stellar population. This effect may be especially important, because the QSO lifetime, the radio source synchrotron lifetime, and the age of the stellar population may be—by selection—of the same order of magnitude, so that a high-redshift QSO may always have a young underlying stellar population.

In conclusion, if high-redshift AGNs reside in young galaxies, the light of their young stars must to some (large) extent affect the UV continuum of lower luminosity AGNs, such as 53W002.

This research was supported by a grant from NASA administered by the American Astronomical Society; NASA *IUE* grants NAG5-547, NAG5-436, and NAG5-1172; NSF grants AST-8821016 and AST-8858203; a Faculty Grant-in-Aid from ASU; a grant from the California Space Institute (CS-77-88); faculty research funds granted by the University of California at Santa Cruz; and the Alfred P. Sloan Foundation.

We thank Jay Gallagher, Anne Kinney, Pat McCarthy, Sumner Starrfield, and Meg Urry for helpful discussions; William Baum for providing us with unpublished color transformations; and Tony Ferro for help in making the figures. We thank the referee, Hy Spinrad, for a careful reading of the manuscript; Gustavo Bruzual for allowing us to use his code; and Stéphane Charlot for help in using the code. We thank Juan Carrasco, Craig Foltz, John McAffee, Janet Robertson, and Skip Staples for assistance at the telescopes, and Gerry Neugebauer for his help in obtaining the IR images. We thank the Netherlands Foundation for Radio Astronomy, NRAO, Whipple Observatory, and NOAO for technical support.

APPENDIX

COMBINATION OF STANDARD STARS IN THE *UBVRI*, *griz*, AND AB_ν SYSTEMS

Here we summarize the transformations used between different photometric systems, since these are crucial for several discussions in the paper. From Oke & Gunn's (1983) definition:

$$AB_\nu(\text{mag}) = -2.5 \log F_\nu(\text{ergs cm}^{-2}\ \text{s}^{-1}\ \text{Hz}^{-1}) - 48.594 \quad \text{(A1)}$$

(please note the typo in the sign of their constant), we can derive fluxes in janskys:

$$F_\nu(\text{Jy}) = 10^{-0.4(AB_\nu - 8.906)}\ , \quad \text{(A2)}$$

once Johnson and Gunn m_λ magnitudes have been converted to AB_ν *magnitudes*. For filters in the Johnson/Mould system (*UBVRIJHK*), m_λ measurements are calibrated with respect to an $m = 0$, A0 V star (with α Lyr as primary standard), so that the corresponding AB_ν magnitudes follow from

$$AB_\nu(\text{mag}) = AB_\nu(\alpha\ \text{Lyr}) + m_\lambda(\text{Johnson}) - m_\lambda(\alpha\ \text{Lyr})\ , \quad \text{(A3)}$$

where $AB_\nu(\alpha$ Lyr) is tabulated in Oke & Gunn (1983), $m_\lambda(\alpha$ Lyr) is a slowly varying but *slightly nonzero* function of wavelength [$m_\lambda(V) = +0.036$ mag for α Lyr (Oke & Gunn 1983); $m_\lambda(J) = m_\lambda(H) = m_\lambda(K) = +0.02$ for α Lyr (Campins, Rieke, & Lebofsky 1985)], and m_λ(Johnson) is the magnitude measured in the Johnson system.

The corresponding AB_ν magnitudes in the Gunn filters follow from m_λ measurements that are calibrated with respect to the primary Gunn standard BD $+17°4708$ (an F6 subdwarf whose spectrum has fewer features than α Lyr and so allows for more accurate calibration):

$$AB_\nu(\text{mag}) = AB_\nu(\text{BD} + 17°) + m_\lambda(\text{Gunn}) - m_\lambda(\text{BD} + 17°)\ , \quad \text{(A4)}$$

where again AB_ν(BD + 17°) are tabulated by Oke & Gunn (1983), while the Gunn m_λ magnitudes for BD $+17°4708$ are $m_\lambda(u) = m_\lambda(v) = m_\lambda(g) = m_\lambda(r) = m_\lambda(i) = m_\lambda(z) = 9.500 \pm 0.001$ mag (Kent 1985), and m_λ(Gunn) is the measured magnitude in the Gunn system.

The resulting constant in equation (A2) depends on wavelength and the spectral type of the primary calibration star. For our filters—Lyα($=4100 \pm 100$ Å FWHM) at the Lick 3 m and Johnson/Mould *UBVRI* at the Steward 90 inch—these constants are (with respect to an $m = 0$, A0 V star) Ly$\alpha = -9.21$, $U = -7.84$, $B = -9.14$, $V = -8.906$, $R = -8.73$, $I = -8.44$, respectively. For Johnson *JHK* and Gunn *griz* at the Palomar 200 inch telescope, these constants are $J = -8.01$, $H = -7.58$, $K = -7.06$ (with respect to an $m = 0$, A0 V star; Campins et al. 1985), and $g = -8.88$, $r = -9.10$, $i = -9.20$, $z = -9.21$ (with respect to an $m = 0$, F6 subdwarf), respectively. The accuracy of these constants depends on how featureless the spectrum is across the passband, ranging from 0.02 mag to $\sim$0.05 mag in redshifted Lyα (4100 Å) and Gunn r (because of nonnegligible Hδ and Hα absorption, respectively).

These relations allow us to predict magnitudes in the Johnson system from the Gunn system—and vice versa—if the spectral type of the object is known. We used this for the calibration of some nonphotometric frames using transfer stars that had accurately measured Gunn colors of F subdwarfs. Identifying these with Oke & Gunn (1983) stars of identical spectral type then allows us to assume identical (Johnson − Gunn) colors, so that combining equations (A3) and (A4) results in

$$m_\lambda(J) = m_\lambda(G) - m_\lambda(G, \text{STD}) + AB_\nu(J, \text{STD}) - [AB_\nu(J, \alpha\ \text{Lyr}) - m_\lambda(J, \alpha\ \text{Lyr})]\ , \quad \text{(A5)}$$

where J indicates the Johnson filter to be calibrated, G indicates a Gunn filter with photometric calibration, and STD indicates one of the Oke and Gunn standards with measured spectral type or Gunn colors identical to the field F subdwarf(s) used as calibration

transfer stars. The relevant AB_ν magnitudes are tabulated for these stars *and* α Lyr in Oke & Gunn (1983); the values of $m_\lambda(G, \mathrm{STD})$ for Gunn standards are given by Kent (1985). The measured magnitudes $m_\lambda(G)$ for field subdwarfs then transform to predicted Johnson magnitudes which should be accurate to 0.05 mag—added in quadrature to the magnitude errors of the calibrated Gunn photometry.

For stars, we can check the above results by inverting the empirical photometric relations of Kent (1985):

$$\text{Johnson } B = \text{Gunn } g + 0.51 + 0.60(g - r) \text{ mag}, \tag{A6}$$

$$\text{Johnson } V = \text{Gunn } g - 0.03 - 0.42(g - r) \text{ mag}, \tag{A7}$$

$$\text{Mould } R = \text{Gunn } r - 0.51 - 0.15(g - r) \text{ mag}. \tag{A8}$$

From the work of Edvardsson & Bell (1989) we arrive at equivalent color transformations, using unpublished color transformations of Baum (1990).

For comparison with the photographic U^+J^+FN system, we combine Kron's (1978) relations [$J^+ = B - 0.23(B-V)$ and $F = V - 0.40(B-V)$] with equations (A6)–(A7) to derive

$$\text{Photographic } J^+ = \text{Gunn } g + 0.39 + 0.37(g - r) \text{ mag}, \tag{A9}$$

$$\text{Photographic } F = \text{Gunn } r - 0.25 + 0.17(g - r) \text{ mag}. \tag{A10}$$

The photographic U and N filters are similar enough to Johnson U and Mould I that we may write

$$\text{Photographic } U^+ \sim \text{Johnson } U \text{ mag}, \tag{A11}$$

$$\text{Photographic } N \sim \text{Mould } I \sim \text{Gunn } i - 0.75 \text{ mag}. \tag{A12}$$

These transformations usually give results consistent within 0.1 mag (§ 2.6), mostly attributable to spectral features within the filter transmission curve, such as the Paschen jump in the Johnson I (but not the Gunn i) filter. The equivalent photographic U^+J^+FN of 53W002 are $U^+ \gtrsim 23.1$, $J^+ = 23.2$, $F = 22.6$, and $N = 22.1$ mag, consistent with 53W002 being just below the 4 m plate limits in the Hercules 2 field (for a compact galaxy like 53W002 these are 0.25–0.5 mag brighter than the stellar plate limits of Windhorst et al. 1984a).

We can now also derive the locus of a power law that involves an unusual combination of Johnson (J) and Gunn (G) filters, such as used in our color-color diagram Figure 6 to locate emission-line objects at 4100 Å. If we define the spectral index in power-law F_ν spectra the usual way,

$$-2.5 \log [F_\nu(J)/F_\nu(G)] = -2.5 \log [\lambda(J)/\lambda(G)]^{+\alpha_0}, \tag{A13}$$

we can combine equations (A3) and (A4) to derive this locus. For Johnson B, Gunn g, and our special redshifted Lyα filter, we then find

$$(4100 \text{ Å} - B) = 0.664(B - g) - 0.10 \text{ mag}. \tag{A14}$$

Values of the spectral index along this locus follow from

$$\alpha_0 = 8.13(B - g) - 2.16. \tag{A15}$$

REFERENCES

Baars, J. W. M., Genzel, R., Pauliny-Toth, I. I. K., & Witzel, A. 1977, A&A, 61, 99
Baldwin, J. A., Wampler, E. J., & Gaskell, C. M. 1989, ApJ, 338, 630
Barbaro, G., & Olivi, F. M. 1989, ApJ, 337, 125
Barthel, P. D. 1989, ApJ, 336, 606
Baum, W. A. 1990, private communication
Bertelli, G., Chiosi, C., & Bertola, F. 1989, ApJ, 339, 889
Bertola, F. 1988, in A Decade of UV Astronomy with the *IUE* Satellite, ed. Y. Kondo (ESA SP-281), 63
Bruzual, G. 1983, ApJ, 273, 105
———. 1989, private communication
Bruzual A., G. 1988, in Astrophysics and Space Science Library, Vol. 141, Towards Understanding Galaxies at Large Redshift, ed. R. G. Kron & A. Renzini (Dordrecht: Kluwer), 161
Burstein, D., & Heiles, C. 1982, AJ, 87, 1165
Burstein, D., Bertola, F., Buson, L. M., Faber, S. M., & Lauer, T. R. 1988, ApJ, 328, 440
Buson, L. M., Bertola, F., & Burstein, D. 1990, in Windows on Galaxies, ed. G. Fabbiano, J. S. Gallagher III, & A. Renzini (Dordrecht: Kluwer), 51
Campins, H., Rieke, G. H., & Lebofsky, M. J. 1985, AJ, 90, 896
Chambers, K. C. 1989, Ph.D. thesis, Johns Hopkins Univ.
Chambers, K. C., & Charlot, S. 1990, ApJ, 348, L1
Chambers, K. C., & McCarthy, P. 1990, ApJ, 354, L9
Chambers, K. C., Miley, G. K., & van Breugel, W. J. M. 1987, Nature, 329, 604
———. 1988, ApJ, 327, L47
———. 1990, ApJ, 363, 21
Cohen, R. D., & Smith, H. E. 1990, in ASP Conf. Ser. Vol. 10, Evolution of the Universe of Galaxies (Edwin Hubble Centennial Symposium), ed. R. G. Kron (Provo, UT: BookCrafters, Inc.), 307
Condon, J. J. 1989, ApJ, 338, 13
Crampton, D., Cowley, A., & Hartwick, F. D. A. 1990, AJ, 100, 47
di Serego Alighieri, S., Fosbury, R. A. E., Quinn, P. E., & Tadhunter, C. N. 1989, Nature, 334, 591
Djorgovski, S. 1988, in Astrophysics and Space Science Library, Vol. 141, Towards Understanding Galaxies at Large Redshift, ed. R. G. Kron & A. Renzini (Dordrecht: Kluwer), 259
Donnelly, R. H., Partridge, R. B., & Windhorst, R. A. 1987, ApJ, 321, 94
Dressler, A., & Gunn, J. E. 1990, in ASP Conf. Ser., Vol. 10, Evolution of the Universe of Galaxies (Edwin Hubble Centennial Symposium), ed. R. G. Kron (Provo, UT: BookCrafters, Inc.), 200
Edvardsson, B., & Bell, R. A. 1989, MNRAS, 238, 1121
Fabian, A. 1989, MNRAS, 238, 41P
Fanaroff, B. L., & Riley, J. M. 1974, MNRAS, 167, 31P
Fitzpatrick, E. L. 1987, ApJ, 312, 596
Foltz, C., Weymann, R., Hazard, C., & Turnshek, D. 1983, PASP, 95, 117
Fomalont, E. B., Windhorst, R. A., Kristian, J. A., & Kellermann, K. I. 1991, AJ, in press
Heisler, J., & Ostriker, J. P. 1988, ApJ, 332, 543
Kapahi, V. K., & Kulkarni, V. K. 1990, AJ, 99, 1397
Keel, W. C., & Windhorst, R. A. 1991, ApJ, in press
Kent, S. M. 1985, PASP, 97, 165
Kinney, A. L., Bohlin, R. C., Blades, J. C., & York, D. G. 1991, ApJS, 75, 645
Kinney, A. L., Huggins, P. J., Bregman, J. N., & Glassgold, A. E. 1985, ApJ, 291, 128
Kinney, A. L., Huggins, P. J., Glassgold, A. E., & Bregman, J. N. 1987, ApJ, 314, 145
Kinney, A. L., Rivolo, A. R., & Koratkar, A. P. 1990, ApJ, 357, 338
Kron, R. G. 1978, Ph.D. thesis, University of California, Berkeley
Kron, R. G., Koo, D. C., & Windhorst, R. A. 1985, A&A, 146, 38
Kwan, J., & Krolik, J. H. 1981, ApJ, 250, 478

Lamb, S. A., Gallagher, J. S., III, Hjellming, M. S., & Hunter, D. A. 1985, ApJ, 291, 63
Le Fèvre, O., Hammer, F., Nottale, L., Mazure, A., & Christian, C. 1988, ApJ, 324, L1
Lilly, S. J. 1988, ApJ, 333, 161
———. 1989, ApJ, 340, 77
———. 1991, private communication
Mathis, D. F. 1991, Master's thesis, Arizona State Univ.
Mathis, D. F., Neuschaefer, L. W., Windhorst, R. A. 1990, BAAS, 22 (No. 2), 888
McCarthy, P. J. 1988, Ph.D. thesis, University of California, Berkeley
———. 1991, private communication
McCarthy, P. J., Spinrad, H., Djorgovski, S. G., Strauss, M. A., van Breugel, W. J. M., & Liebert, J. 1987, ApJ, 319, L39
McCarthy, P. J., Kapahi, V. K., van Breugel, W. J. M., & Subrahmanya, C. R. 1990a, AJ, 100, 1014
McCarthy, P. J., Spinrad, H., van Breugel, W., Liebert, J., Dickinson, M., Djorgovski, S., & Eisenhardt, P. 1990b, ApJ, 365, 487
Neuschaefer, L. W., Windhorst, R. A., & Dressler, A. 1991, ApJ, in press
Oke, J. B., & Gunn, J. E. 1983, ApJ, 266, 713
Oort, M. J. A. 1987, Ph.D. thesis, University of Leiden
Oort, M. J. A., Katgert, P., Steeman, F. W. M., & Windhorst, R. A. 1987, A&A, 179, 41
Oort, M. J. A., & van Langevelde, H. J. 1987, A&AS, 71, 25
Panek, R. J., & Savage, B. D. 1976, ApJ, 206, 167
Prinja, R. K. 1990, MNRAS, 246, 392
Scalo, J. M. 1986, Fund. Cosmic Phys., 11 (No. 1), 278
Scarrot, S. M., Rolph, C. D., & Tadhunter, C. N. 1990, MNRAS, 243, 5P
Seaton, M. J. 1979, MNRAS, 187, 73P
Underhill, A. B. 1982, in Monograph Series on Nonthermal Phenomena in Stellar Atmospheres, ed. A. Underhill & V. Doazan (NASA SP-456), 62
Underhill, A. B., Leckrone, D. S., & West, D. K. 1972, ApJ, 171, 63
Wampler, E. J., Gaskell, C. M., Burke, W. L., & Baldwin, J. M. 1984, ApJ, 276, 403
Wild, J. P. 1970, Australian J. Phys., 23, 113
Windhorst, R. A. 1984, Ph.D. thesis, Univ. Leiden
———. 1986, in Highlights Astr., Vol. 7, ed. J.-P. Swings (Dordrecht: Reidel), 355
Windhorst, R. A., Dressler, A., & Koo, D. C. 1987, in IAU Symposium 124, Observational Cosmology, ed. A. Hewitt, G. Burbidge, & L. Z. Fang (Dordrecht: Reidel), 573
Windhorst, R. A., Kron, R. G., & Koo, D. C. 1984a, A&AS, 58, 38
Windhorst, R. A., Mathis, D. F., & Neuschaefer, L. W. 1990, in ASP Conf. Ser., Vol. 10, Evolution of the Universe of Galaxies (Edwin Hubble Centennial Symposium), ed. R. G. Kron (Provo, UT: BookCrafters, Inc.), 389
Windhorst, R. A., Miley, G. K., Owen, F. N., Kron, R. G., & Koo, D. C. 1985, ApJ, 289, 494
Windhorst, R. A., & Oppe, J. 1991, A&AS, submitted
Windhorst, R. A., van Heerde, G. M., & Katgert, P. 1984b, A&AS, 58, 1
Wyse, R. F. G. 1985, ApJ, 299, 593